

2 **Using hydrologic landscape classification and climatic time series**
3 **to assess hydrologic vulnerability of the Western U.S. to climate**

4 Chas E. Jones Jr.^{1*}, Scott G. Leibowitz², Keith A. Sawicz³, Randy L. Comeleo², Laurel E.
5 Stratton⁴, Phillip E. Morefield⁵, Chris P. Weaver⁶

6 ¹ Oak Ridge Institute for Science and Education (ORISE), c/o U.S. Environmental Protection Agency, Center for
7 Public Health and Environmental Assessment, Pacific Ecological Systems Division, 200 SW 35th St., Corvallis, OR
8 97333, USA; Current affiliation: Affiliated Tribes of Northwest Indians, Corvallis, OR 97333, USA
9

10 ² U.S. Environmental Protection Agency, Center for Public Health and Environmental Assessment, Pacific Ecological
11 Systems Division, 200 SW 35th St., Corvallis, OR 97333, USA
12

13 ³ Oak Ridge Institute for Science and Education (ORISE), c/o U.S. Environmental Protection Agency, Center for
14 Public Health and Environmental Assessment, Pacific Ecological Systems Division, 200 SW 35th St., Corvallis, OR
15 97333, USA; Current Affiliation: AIR Worldwide, 131 Dartmouth Street #4, Boston, MA 02116, USA
16

17 ⁴ c/o U.S. Environmental Protection Agency, Center for Public Health and Environmental Assessment, Pacific
18 Ecological Systems Division, 200 SW 35th St., Corvallis, OR 97333, USA
19

20 ⁵ U.S. Environmental Protection Agency, Center for Public Health and Environmental Assessment, Health and
21 Environmental Effects Assessment Division, Washington, DC 20460, USA
22

23 ⁶ U.S. Environmental Protection Agency, Center for Public Health and Environmental Assessment, Health and
24 Environmental Effects Assessment Division, Research Triangle Park, NC 27709, USA

25 *Correspondence to:* Chas E. Jones Jr. (chas@chasjones.com)

26 **Abstract.** We apply the hydrologic landscapes (HL) concept to assess the hydrologic vulnerability of the western
27 United States (U.S.) to projected climate conditions. Our goal is to understand the potential impacts of hydrologic
28 vulnerability for stakeholder-defined interests across large geographic areas. The basic assumption of the HL approach
29 is that catchments that share similar physical and climatic characteristics are expected to have similar hydrologic
30 characteristics. We use the Hydrologic Landscape vulnerability approach (HLVA) to map the HLVA index (an
31 assessment of climate vulnerability) by integrating the HL approach into a retrospective analysis of historical data to
32 assess variability in future climate projections and hydrology, which includes temperature, precipitation, potential
33 evapotranspiration, snow accumulation, climatic moisture, surplus water, and seasonality of water surplus. Projections
34 that are beyond two-standard deviations of the historical decadal average contribute to the HLVA index for each
35 metric. Separating vulnerability into these seven separate metrics allows stakeholders and/or water resource managers
36 to have a more specific understanding of the potential impacts of future conditions. We also apply this approach to
37 examine case studies for particular locations. The case studies (Mt. Hood, Willamette Valley, and Napa-Sonoma
38 Valley) are important to the ski and wine industries and illustrate how our approach might be used by specific
39 stakeholders. The resulting vulnerability maps show that temperature and potential evapotranspiration are consistently
40 projected to have high vulnerability indices for the western U.S. Precipitation vulnerability is not as spatially uniform
41 as temperature. The highest elevation areas with snow are projected to experience significant changes in snow
42 accumulation. The seasonality vulnerability map shows that specific mountainous areas in the West are most prone to
43 changes in seasonality, whereas many transitional terrains are moderately susceptible. This paper illustrates how HL
44 and the HLVA can help assess climatic and hydrologic vulnerability across large spatial scales. By combining the HL
45 concept and HLVA, resource managers could consider future climate conditions in their decisions about managing
46 important economic and conservation resources.

47 **1 Introduction**

48 A stable and predictable water supply is imperative for food security, ecosystem sustainability, economic stability,
49 and even national security (National Intelligence Council, 2012), and is related the threats of increased flooding,
50 droughts, wildfire, and more extreme temperatures (Mancosu et al., 2015; Mekonnen and Hoekstra, 2016). The
51 recognition of the potential socio-ecological threats of climate change on the water supply is a critically important
52 topic, and the development of planning tools that identify vulnerabilities to these systems could help decision-makers
53 assess the risks of environmental changes imposed by climate as well as other contemporary risks (e.g., population
54 growth and habitat conversion) (Glick et al., 2011; Lawler et al., 2010). Climatic and hydrologic change will not
55 impact stakeholders equally across sectors, thus the specific concerns and adaptation strategies of different industries
56 threatened by those risks will vary. The hydrologic landscapes vulnerability assessment described herein provides a
57 relatively simple approach for assessing hydrologic vulnerability based upon inferences of hydrologic behavior (using
58 hydrologic landscapes) in response to climatic impacts. This approach can be applied across large geographic regions
59 and can potentially benefit numerous sectors, including environmental, economic, and other ecosystem services.

60 Numerous studies have examined projected changes in climate and hydrology on regional and national scales that
61 included the western United States (U.S.). The Fourth National Climate Assessment is a comprehensive resource for
62 climate-related research in the U.S. (U.S. Global Change Research Program (USGCRP), 2018). Nolin and Daly (2006)
63 mapped climate-related risk to snow-dominated areas and ski areas in the Pacific Northwest (PNW, which includes
64 Washington, Oregon, and Idaho). Mote et al. (2005) compared the spatial patterns of snow water equivalent
65 observations to model simulations in the western U.S. Brown and Mote (2009) examined projected changes in snow
66 water equivalent globally based on 14 model projections. Barnett et al. (2005) identified potential climate-driven water
67 supply deficits in snow-dominated areas around the globe, although rising water demands have been found to greatly
68 outweigh potential climate impacts on future (year 2025) water supply (Vorosmarty et al., 2000). McAfee (2013)
69 examined projected changes in potential evapotranspiration (PET, calculated using numerous methods) and found
70 regional analyses to be more inconsistent than studies across the conterminous U.S., which indicated sensitivities to
71 the methods used. Hill et al. (2013, 2014) predicted thermal vulnerability of streams and river ecosystems to climate
72 across the U.S., while Battin et al. (2007) found that salmon habitat in snow-dominated streams was more vulnerable
73 than habitat in lowland streams. The analyses of Nijssen et al. (2001) on hydrologic sensitivity of rivers globally
74 found: 1) ubiquitous warming, with greatest warming in winter months at higher latitudes, 2) more precipitation with
75 high variability, 3) early to mid-spring snowmelt caused increased spring streamflow peak in coldest basins, decreased
76 spring runoff and increased winter runoff in transitional basins, 4) tropical or mid-latitude basins had decreased annual
77 runoff, and 5) high latitude basins had increased annual streamflow. While snow-fed streams in the western US seem
78 less likely to change flow regimes, perennial and intermittent, rain-fed streams are more likely to change in flow
79 regime (Dhungel et al., 2016). In response to droughts of the recent past, Mann and Gleick (2015) highlight the strong
80 correlation between very hot years and very dry years; thus as temperatures increase at the upper extreme, precipitation
81 is becoming more scarce. A study by Cook et al. (2015) found a growing risk of unprecedented drought in the western
82 U.S. based on temperature projections and no clear pattern in future precipitation.

83 “Vulnerability” has been defined in many ways, depending upon discipline and application (Adger, 2006; Füssel,
84 2007). Vulnerability assessments often integrate exposure, sensitivity, and adaptive capacity to stressors (Adger, 2006;
85 Füssel, 2007; Füssel and Klein, 2006; IPCC, 2014). Researchers have studied vulnerability at varying scales across
86 numerous regions for a diversity of stakeholders, and they tend to focus on the most relevant metrics for their particular
87 application (Farley et al., 2011; Glick et al., 2011; IPCC, 2014; Nolin and Daly, 2006; U.S. Global Change Research
88 Program, 2011; Watson et al., 2013). Yet, better products and services are needed to enable local communities to plan
89 for and respond to hydrologic change, which includes services that improve understanding, observing, forecasting,
90 and warning about significant hydrologic events (Tansel, 2013). Glick et al. (2011) and Lawler et al. (2010) both
91 emphasize the importance to managers of understanding the potential impacts of climate on the resources that they
92 manage.

93 There have been many efforts to assess hydrologic vulnerability related to specific stakeholders, ecosystems, or
94 locations. For example, Vörösmarty et al. (2000) examined the vulnerability of global water resources to changes in

95 climate and population growth. Hill et al. (2014) assessed stream temperature vulnerability to climate for sites across
96 the U.S. In another example, Winter (2000) suggested that the vulnerability of wetlands to changes in climate depends
97 upon their position within the hydrologic landscape.

98 There are opportunities to build upon previous efforts to map hydrologic vulnerability across large geographic areas,
99 while creating tools that stakeholders may use to understand the potential impacts for their asset of interest in specific
100 watersheds. Winter (2001) described the concept of classifying the physical landscape and climatic properties of large
101 landscape units based on hydrologic landscapes (HL). Surface and ground water availability in watersheds is impacted
102 by differences in geology, terrain, soils, seasonal temperature patterns, precipitation magnitude, and precipitation
103 timing (Tague et al., 2013; Winter, 2001) and are not uniform across regions (Hamlet, 2011; Jung and Chang, 2012;
104 Tague and Grant, 2004). Catchments that share similar key physical and climatic characteristics are expected to have
105 similar hydrologic characteristics; i.e., surface and ground water interactions, deposition, timing, and accumulation of
106 precipitation, surface runoff patterns, and groundwater flow (Nolin, 2011; Thompson and Wallace, 2001).

107 The HL concept has been applied to the U.S. using a clustering method (Wolock et al., 2004) to develop twenty non-
108 contiguous regions, which were much larger than the catchment scale. Since that effort, modified approaches have not
109 used clustering approaches, but have used catchment-based classification in Oregon (Leibowitz et al., 2014; Patil et
110 al., 2014; Wigington et al., 2013), Nevada (Maurer et al., 2004), the PNW (Comeleo et al., 2014; Leibowitz et al.,
111 2016), and Bristol Bay, Alaska (Todd et al., 2017). In applying the HL approach in Oregon and the PNW, the clustering
112 approach was abandoned for a conceptual approach based upon important factors known to contribute to hydrologic
113 flow (Wigington et al., 2013), where two climatic factors and three landscape characteristics were categorized for each
114 catchment; the resulting classification allows the estimation of catchment-scale hydrologic behavior across large
115 spatial scales. The approach shows promise in predicting seasonal and monthly hydrologic patterns (Leibowitz et al.,
116 2014). Leibowitz et al. (2014) adapted the classification system applied by Wigington et al. (2013) to illustrate the
117 applicability of HLs at the watershed scale for representing normal (1971-2000) monthly average streamflow in three
118 case study watersheds in Oregon. They used climate projections (2041-2070) to estimate hydrologic behavior of
119 watersheds relative to 1971-2000. Leibowitz et al. (2016) expanded the approach and applied the HL classification to
120 Oregon, Washington, and Idaho. The more recent studies using the hydrologic landscape classification approach have
121 been applied at a watershed scale (Patil et al. 2014, Leibowitz et al. 2016, Todd et al. 2017).

122 A number of tactics have been used to investigate the influence of climate on hydrologic behavior (Luce and Holden,
123 2009; Safeeq et al., 2014; Vano et al., 2015). To extend the work previously completed from HL-based climate
124 projections, we assess hydrologic vulnerability at the catchment scale by integrating the HL approach into an analysis
125 of climatic variability. Our hydrologic landscape vulnerability approach (HLVA) provides spatially continuous,
126 application-specific estimates of climatic vulnerability (maps of the HLVA indices). One of the benefits of the HLVA
127 is to place recent and projected environmental changes in the context of available historic data. In the HLVA, we use
128 proxies for the three components of vulnerability: a) historic climate data and their derivatives as proxies for sensitivity
129 (the sensitivity of a particular system to each variable); b) climate projections as proxies for exposure (the future

130 projected condition increases or decreases a system's exposure to a change); and c) qualitative considerations of
131 ecosystems, stakeholders, or industries as proxies for adaptive capacity (the presence of a system in a location is
132 indicative that the system has historically had sufficient adaptive capacity to exist in that area). Using HLVA, we
133 examine vulnerability to changes in temperature, precipitation, potential evapotranspiration, snow accumulation,
134 surplus water, climatic moisture, and seasonality of the water surplus. This method highlights areas that are projected
135 to experience deviations from historic conditions to understand the patterns in magnitude, timing, and type of
136 precipitation and the quantity and seasonality of available water at a catchment scale. These estimates of hydrologic
137 vulnerability could offer important insight into the potential resilience of socially and economically valuable locations
138 and stakeholders in an area.

139 We assess the hydrologic vulnerability of socially and economically valuable locations by applying the HL concept
140 using climatic projections in the western U.S. We analyzed the output from the HL analyses to address three research
141 objectives: 1) develop an index of vulnerability based on climate; 2) map areas that are projected to be more vulnerable
142 to environmental change; and 3) determine the vulnerability indices for socially and economically valuable locations,
143 including three example case studies for regional industries that are economically important in the region. By
144 integrating the concept of hydrologic landscape classification, hydrologic vulnerability, and climatic impacts, this
145 study lays the groundwork for making spatially explicit generalizations about the hydrologic vulnerability of socially
146 and economically valuable locations across large landscapes.

147 **2 Methods**

148 **2.1 Study Area**

149 The study area includes the states of Washington, Oregon, Idaho, California, Nevada, and Arizona in the western U.S.
150 (Fig. 1). These states extend across a wide range of climates and diverse physiographic settings. The lowest elevation
151 across the six states is 85 m below sea level (Death Valley, California), while the highest elevation is 4421 m above
152 sea level (Mt. Whitney, California) [U.S.G.S. National Elevation Dataset available at:
153 <https://nationalmap.gov/elevation.html>]. The Sierra-Nevada Mountains are oriented in a north-south direction near the
154 eastern border of California and transition to the Cascade mountain range that is oriented north-south through Oregon
155 and Washington (US Topo Quadrangles available at: <https://nationalmap.gov/ustopo>). There are numerous other
156 mountain ranges in the other states as well. The Sierra-Nevada and Cascade mountain ranges generate orographic
157 effects that cause upwind areas to the west to have greater precipitation relative to the downwind, eastern regions
158 (Dettinger et al., 2004; Siler et al., 2013). High elevation areas receive most of their precipitation as snow (Brekke et
159 al., 2009; Mote et al., 2005), while lowland and coastal areas receive predominantly rain (Brekke et al., 2009; Mock,
160 1996), but much of the study area receives a balance of snow and rain. The topographic differences drive precipitation
161 patterns across the area and cause differences in the total annual precipitation or the seasonality of maximum
162 precipitation (Mock, 1996). In the arid southwest, summer monsoons deliver most of the annual precipitation, whereas
163 in the PNW, winter rains and snows prevail (Mock, 1996). However, the western U.S. is regularly affected by

164 atmospheric rivers that deliver large quantities of rain or snow over short periods (Dettinger, 2011; Hidalgo et al.,
165 2009). The seasonal variability of surface air temperature varies widely across the study area. Portions of each state
166 are classified as deserts with summer maximum temperatures regularly exceeding 40°C (NOAA State Climate
167 Extremes Committee, 2016). Each state has also recorded temperatures less than -40°C (NOAA State Climate
168 Extremes Committee, 2016). Some areas have mild climates with little seasonal variation in temperature (Daly,
169 2016b). Geology in the study area varies from high permeability sedimentary deposits or relatively recent volcanic
170 deposits, to low permeability igneous metamorphic and sedimentary formations and older volcanics (Comeleo et al.,
171 2014; Stratton et al., 2016).

172 **2.2 Hydrologic landscape classification**

173 Assessment units (AUs) are aggregations of NHDPlusV2 catchments (McKay et al., 2012) that were grouped to have
174 a target area of 80 km², as described in Leibowitz et al. (2016). In this study, the same assessment units used in
175 Leibowitz et al. 2016 study have been used and their method applied to the expanded six state study region to delineate
176 29,097 assessment units for the study's expanded 6 state study region. For this analysis, we retain an AU if its centroid
177 was located within the boundary of our project area or if the AU extended across an international boundary. All AU
178 polygons are clipped to the international boundary of the U.S. These conditions allow us to avoid edge effects at
179 international and state borders by avoiding overlapping AUs at state boundaries and analyzing the HLs up to all
180 international borders.

181 Building upon Winter's (2001) approach and the Wolock et al. (2004) clustering approach, Wigington et al. (2013)
182 developed their simple conceptual HL classification based on climatic and physical characteristics of the physical
183 watershed. They combined five indices related to hydrologic flow (Fig. 2a) to characterize the major drivers that
184 control the magnitude and timing of water movement through the landscape and into the groundwater or stream
185 network: (1) climate, which describes the overall water availability, (2) seasonality of water surplus, which is the
186 season when the maximum excess of water is available to infiltrate into the soil or flow as surficial runoff, (3)
187 subsurface permeability, (4) terrain, and (5) surface permeability. Note that Wigington et al. (2013) referred to
188 subsurface and surface permeability as aquifer and soil permeability, respectively. The five HL indices, described in
189 more detail below (Sections 2.2.1 through 2.2.5), are concatenated into a 5-character HL code (e.g., WsLMH, SwHTh,
190 or DfHfL) that characterizes an AU.

191 Leibowitz et al. (2016) modified the Wigington et al. (2013) approach by including: the use of assessment units based
192 on National Hydrography Dataset Plus V2 catchments, a modified snowmelt model that was validated over a broader
193 area, a subsurface permeability index that does not require pre-existing aquifer permeability maps, and a surface
194 permeability threshold based on objective criteria. Using this modified method (herein described as the modified
195 Wigington et al. (2013) approach), they developed an HL map of the PNW. Here, we used the modified Wigington et
196 al. (2013) approach to develop an HL classification of California, Nevada, and Arizona. This was then combined with
197 the PNW map (Leibowitz et al., 2016) to create an HL map of the study area.

198 **2.2.1 Climate**

199 The Wigington et al. (2013) approach derived the climate index from the Feddema Moisture Index (FMI) (Feddema,
200 2005):

201
$$FMI = \begin{cases} 1 - \frac{PET}{P} & \text{if } P \geq PET \\ \frac{P}{PET} - 1 & \text{if } P < PET \end{cases} \quad (1)$$

202 where FMI (Eq. (1)) values range from -1.0 (arid) to 1.0 (very wet). P is the mean precipitation (mm) over a 30-year
203 period, which is derived from climate data described in Section 2.3, and PET is the potential evapotranspiration (mm)
204 calculated using the Hamon (1961) method, that utilizes mean daily temperature, daytime length (calculated based on
205 latitude), and a calibration coefficient. The range of FMI values was the basis for defining a climate index consisting
206 of six classes: arid (A; $-1.0 \leq FMI < -0.66$), semiarid (S; $-0.66 \leq FMI < -0.33$), dry (D; $-0.33 \leq FMI < 0.0$), moist (M;
207 $0.0 \leq FMI < 0.33$), wet (W; $0.33 \leq FMI < 0.66$), and very wet (V; $0.66 \leq FMI < 1.0$) (Wigington et al., 2013). FMI
208 was calculated from regional precipitation rasters (described in Section 2.3) for each period of interest. The FMI value
209 was then averaged over each AU.

210 **2.2.2 Seasonality**

211 We used the Leibowitz et al. (2016) approach to develop a seasonality index that identifies the season of the maximum
212 monthly average snowpack-corrected surplus water (S'_m):

213
$$S'_m = S_m - \Delta PACK_m^*$$

214
$$S'_m = (P_m - PET_m) - (PACK_m^* - PACK_{m-1}^*) \quad (2)$$

215 where S'_m (Eq. (2)) is the average snowpack-corrected water surplus (mm) for month m , S_m is monthly water surplus
216 ($P - PET$), and P_m and PET_m are monthly precipitation and monthly PET, respectively. $PACK_m^*$ is a monthly bias-
217 corrected snowpack value (in mm of snow water equivalent, or SWE) restricted to values greater than zero, based on
218 the Leibowitz et al. (2016) modifications to the Leibowitz et al. (2012) snowpack model. Note that $\Delta PACK_m^*$ can have
219 negative values, which represents snow melt. For each month, S'_m was calculated for the regional raster, before
220 identifying the month of maximum S'_m for the majority of pixels in each AU. The month of maximum S'_m was used
221 to identify the season of maximum S'_m based upon four seasonality classes: fall (f; October–December), winter (w;
222 January–March), spring (s; April–June), and summer (u; July–September). The PNW analysis by Leibowitz et al.
223 (2016) only included two seasonality classes; summer seasonality did not occur, while fall and winter were combined
224 into a winter class, since this represented the PNW's wet season. For this analysis, winter and fall were separated and
225 all four seasonality classes were used, because fall and winter are distinct seasons in other parts of the nation.

226 **2.2.3 Subsurface permeability**

227 Leibowitz et al. (2016) utilized the Comeleo (2014) aquifer permeability dataset. We applied a similar approach to the
228 Stratton et al. (2016) aquifer permeability datasets, which is herein referred to as subsurface permeability. Each dataset
229 classifies the subsurface permeability into high (H) and low permeability (L) classes, which are assigned with a
230 threshold of $8.5 \times 10^{-2} \text{ m day}^{-1}$ hydraulic conductivity. Using these data, we analyzed the subsurface permeability of
231 each AU by identifying the subsurface permeability class for the majority of pixels within each AU in California,
232 Nevada, and Arizona.

233 **2.2.4 Terrain**

234 To classify terrain, we used the same approach as Wigington et al. (2013). We analyzed a 30 m Digital Elevation
235 Model to classify the landscape based upon the topographic characteristics of each AU. “Mountainous” (M) areas had
236 AUs with <10 % of the area identified as flat (< 1 % slope) and greater than 300 m of total relief. AUs with more than
237 50 % area having < 1 % slope were classified as “flat” (F). All other AUs were identified as “transitional” (T).

238 **2.2.5 Surface permeability**

239 For surface permeability, the Leibowitz et al. (2016) HL approach utilized the STATSGO soil permeability raster
240 developed by Pennsylvania State University Center for Environmental Informatics (www.cei.psu.edu) for the top 10
241 cm of soil (Miller and White, 1998) in the conterminous U.S. The STATSGO soils database was selected because of
242 its complete coverage of the conterminous U.S., despite SSURGO’s higher spatial resolution, yet incomplete coverage
243 of the study area. Leibowitz et al. (2016) identified whether the majority of each AU had high (H; $>1.52 \text{ cm/hr}$) or
244 low (L; $\leq 1.52 \text{ cm h}^{-1}$) soil permeability. We applied the same approach to classify surface permeability of each AU
245 into two classes throughout the region.

246 **2.3 Climate analyses**

247 **2.3.1 Climate normal (1971–2000)**

248 The climate normal was defined as the 1971-2000 period to align with the Leibowitz et al. (2016) study. Average
249 monthly precipitation and mean temperature were acquired from Parameter-elevation Regressions on Independent
250 Slopes Model (PRISM; Daly, 2016b) data for our normal climatic period at a resolution of approximately 400 m. The
251 PRISM Climate Mapping Program is an ongoing effort to produce detailed, spatial climate datasets (Daly, 2016a;
252 Daly et al., 2000). PRISM uses point measurements of climate data and a digital elevation model to map climate across
253 the U.S. from 1895–present, including regions impacted by high mountains, rain shadows, temperature inversions,
254 coastal regions, and associated complex meso-scale climate processes. Using ArcGIS (ESRI, 2016), the data were
255 clipped to the project boundary and used to calculate the average for seven metrics: monthly temperature ($^{\circ}\text{C}$),
256 precipitation (mm), PET (mm), surplus water (mm), snow water equivalent (mm), the FMI climate index (unitless),
257 and seasonality of water surplus (unitless). Each metric is an input to or products of the HL classification process.

258 **2.3.2 Historical climate analyses (1901–2010)**

259 Unlike the 1971-2000 monthly precipitation and temperature data, a time series of gridded monthly historical climate
260 data at a spatial resolution of 400 m was not available without paying a fee. However, daily PRISM data were freely

261 available at 4 km resolution, so we used these to develop the historical climate analyses for the 1901–2010 period.
262 These gridded data for daily mean temperature and precipitation were clipped to the project boundary and averaged
263 for each month over each decade (i.e., 1901–1910, 1911–1920, etc.). The data were then statistically downscaled to
264 400 m using the delta method (Hijmans et al., 2005; Ramirez-Villegas and Jarvis, 2010) to match the spatial and
265 temporal resolution of the climate normal data (using the 400 m resolution, monthly PRISM climate normal for 1971–
266 2000 period as the high resolution dataset). We acknowledge the inaccuracies and uncertainty imposed in the
267 temperature and precipitation datasets by applying the downscaling functions to the original climate projections. While
268 the 400m data clearly have greater resolution and less error than the 4km data, these data were to be aggregated to
269 assessment units with a mean area of 56 km². In practice, the larger 4km resolution of the downscaled historical
270 analysis should still be appropriate for the scale of the assessment units, thus the trade-offs were deemed acceptable
271 and preferable for characterizing the hydrology and climate for these analyses with no additional budget requirements.

272 Based on the approaches described, the downscaled data were used to calculate the average monthly PET, surplus
273 water, snow water equivalent, FMI, and seasonality of water surplus for each decade (Fig. 2b). Summary figures were
274 generated from this data depicting spatial distribution of climate and seasonality for each decade across the project
275 area. These data were compared to the climate normals using spatially continuous time series analyses (Fig. S1).

276 **2.3.3 Future climate analyses (2041–2070)**

277 In order to explore the potential range of modeled climatic response for the study area, we selected ten climate model
278 projections from the full ensemble of World Climate Research Programme’s Coupled Model Intercomparison Project
279 phase 5 multi-model ensemble climate dataset projections (WCRP CMIP5; <http://cmip-pcmdi.llnl.gov/cmip5>; Taylor
280 et al., 2012). These models are based on the Representative Concentration Pathway (RCP) 8.5 emissions scenario,
281 which assumes the highest rate of emissions into the 21st century and most closely relates to conditions observed to
282 date (Schwalm et al., 2020). To reduce the complexity of the analyses, we used only this one emissions scenario. To
283 select the specific model simulations to use in this study, we used the U.S. Environmental Protection Agency’s (EPA)
284 LASSO tool (lasso.epa.gov; U.S. EPA, 2020) to generate a scatterplot comparing future temperature and precipitation
285 change for the different CMIP5 models over the project area. Using the scatterplot and the approach described by U.S.
286 EPA (2020), we subjectively selected ten models that spanned the entire range of predicted climatic responses of the
287 full ensemble in a distributed manner (Fig. 3), including drier, wetter, colder, and warmer responses. Average monthly
288 precipitation and temperature for the ten projections (Table 1) were acquired from the monthly Bias-Correction and
289 Spatial Disaggregation (BCSD) archive (Bureau of Reclamation, 2014) for the 2041–2070 period. These data were
290 clipped to the project boundary and resampled to a 400 m grid using a bilinear approach (ESRI ArcGIS v10.4) to
291 match the resolution and spatial extent of the climate data. The average monthly PET, surplus water, snow water
292 equivalent, FMI, and seasonality of water surplus were calculated from the future climate data for each assessment
293 unit. Example figures were generated that illustrate the spatial distribution of the differences in FMI (Fig. S1 and S2)
294 and seasonality of water surplus (Fig. S3 and S4) from the normal period for each climate projection (Fig. 2c).

295 **2.4 Mapping vulnerability indices**

296 As discussed in the introduction, vulnerability can be measured by assessing the *exposure*, *sensitivity*, and *adaptive*
297 *capacity* of a system to change (Adger, 2006; Füssel, 2007; Füssel and Klein, 2006; IPCC, 2014). Hydrology and
298 climate are primary forcing factors for ecosystems (Nelson, 2005) and are critical to certain industries and stakeholders
299 in particular areas, and thus analyses of historic variation in hydrology and climate in an area can serve as proxies for
300 the historical *sensitivity* of those systems to environmental change. Likewise, we used future climate projections as a
301 proxy for *exposure*. Projections that fell outside of historic observations were assumed to be associated with increased
302 exposure to the forcing factors for environmental change, which include hydrology and climate. In terms of *adaptive*
303 *capacity*, we assumed that the systems present in a location are adapted to the historic variability in conditions. We
304 also assumed that the systems would become stressed by conditions far outside of those previously experienced.
305 Further, we suggest that the greater the number of future climate projections that exceed or fall far below the historic
306 range, the more vulnerable a system will be with respect to climate-induced changes. Thus, HLVA places projected
307 environmental changes in the context of historic trends. The HLVA assesses vulnerability to changes in temperature,
308 precipitation, potential evapotranspiration, surplus water, snow accumulation, climatic moisture, and seasonality of
309 the water surplus by identifying areas that are projected to experience future deviations from historic conditions (Fig.
310 2e).

311 The ten future climate projections (for the 2041–2070 period) were compared to the decadal averaged data from 1901–
312 2010 for each AU. We calculated the historical standard deviation of each metric for each AU within the project area.
313 For each metric, we assume that any projection within two-standard deviations of the historical climate values does
314 not contribute to an increase in vulnerability, whereas projections outside of that range increase the vulnerability. We
315 then define vulnerability for a given metric as the number of the ten projections that are outside of the historical two-
316 standard deviation threshold. Thus, the HLVA index assesses the likelihood that a given metric will exceed a two-
317 standard deviation threshold from the decadal mean under future climate scenarios. Because individual models exceed
318 the threshold of two standard deviations from the mean in both the higher and lower directions, there is not a unique
319 direction of change associated with the vulnerability index. Thus, the vulnerability index, as defined, does not convey
320 information about projected direction of change. A vulnerability index of ten indicates that all ten climate projections
321 were beyond two-standard deviations from the historical mean and that the area is expected to experience projected
322 conditions that it is not adapted to. The least vulnerable areas will have an index of zero, which indicates that all future
323 climate projections fell within the two-standard deviation threshold to which systems are adapted to. The use of
324 standard deviations is not an appropriate threshold metric for seasonality, because it is a categorical variable. For the
325 seasonality metric, any projected seasonality value that has not been observed decadal between 1900 and 2010
326 increases the seasonality vulnerability index. For example, consider an AU that had predominantly experienced spring
327 seasonality, with the occasional fall seasonality, and that 7 of 10 climate models project fall seasonality and 3 of 10
328 models predict winter seasonality for 2041–2070. Since winter seasonality was not observed for any decade between
329 1900 and 2010, the three predictions for winter seasonality would contribute to a vulnerability index of three for
330 seasonality in that case. Finally, we analyzed the dominant HL code by area of the most vulnerable AUs (those having

331 a vulnerability index greater than seven on a scale of ten) for each metric in order to gain insight about the dominant
332 HL characteristics that relate to hydrologic vulnerability.

333 **2.5 Locational time series analyses**

334 Forty-five locations (Fig. 1 and Table 2) were selected for potential applications of the HL approach to demonstrate
335 the method's relevance to potential water resource stakeholders to identify areas where we thought results could be of
336 use to land managers. Specific sites were selected subjectively so that we could examine representative climate impacts
337 at sites that may be of general interest. These sites include cities, national parks, mountains, national forests, and areas
338 with hydrologically sensitive economic interests. AUs were used to represent a geographic feature if its centroid was
339 located within the geographic boundary of a location of interest. The location boundary was defined by merging these
340 AUs into a single polygon. For instance, the Great Basin National Park (GBNP) was covered by a single AU, rather
341 than numerous AUs because the centroid of only one AU was within the park boundary, whereas all other AU centroids
342 were located outside of the GBNP boundary. The time series for the decadal averages for each of the climate-related
343 HL metrics were analyzed for the AUs associated with each location. Decadal averages were plotted at the decadal
344 midpoint for each 10-year period from 1901 to 2010. In addition, the 1971–2000 normal average for each variable
345 and ten climate projections (2041–2070) were also plotted. The HLVA was then used to determine the mean
346 vulnerability index and the dominant HL code for the AUs associated with each location (Fig. 2d).

347 **3 Results**

348 **3.1 Hydrologic landscape summary**

349 Table 3 shows the percent coverage of the HL categories for the six states. Thirty percent of the region is mountainous
350 (elevation relief of AU > 300 m and < 10 % of AU area has slope < 1 %) and 7 % is flat (AUs with more than 50 %
351 area having < 1 % slope). The remaining area is classified as transitional. According to the soil permeability dataset
352 (Miller and White, 1998) produced from the STATSGO soils database (Soil Survey Staff, 2016), 98 % of the surface
353 soils (defined as the top 10 cm) are highly permeable (> 4.23 $\mu\text{m s}^{-1}$). Stratton et al. (2016) and Comeleo et al. (2014)
354 classified the subsurface permeability of the six-state region as 60 % high permeability and 40 % low permeability.
355 During the 1971–2000 climate normal period, most of the area has the highest monthly water availability (seasonality)
356 during the winter (63 %), followed by 24 % of the area showing fall seasonality, 13 % having spring seasonality, with
357 only 1 % experiencing summer seasonality. In addition, 30 % of the area is classified as having a moist, wet, or very
358 wet climate, while 70 % is dry, semi-arid or arid. The HL maps for the study area are included in the appendix (Fig.
359 A1). HL maps for the remainder of the conterminous U.S. are also available and are included as supplemental material
360 (Fig. S6; although subsurface permeability maps are not available for all of the lower 48 states).

361 **3.2 Climate Vulnerability analyses**

362 Using the analyses of historic and future climate, the vulnerability indices were mapped for all seven metrics
363 (examples are provided for FMI and seasonality in the supplemental materials). The vulnerability maps (Fig. 4)
364 identify areas that are subject to extreme future climatic and hydrologic variability (similar vulnerability maps for the
365 conterminous U.S. are included in the supplemental materials (Fig. S6)). Note that while it is possible to evaluate

366 direction of change (greater or less than two standard deviations) for the projection of an individual climate model,
367 the vulnerability index is the integration of ten individual models. Therefore, it is possible for individual models to
368 exceed the threshold of two standard deviations from the mean in either the higher or lower directions; thus there is
369 not a unique direction of change associated with our vulnerability index as it has been defined.

370 All climate projections indicate that temperature will change almost ubiquitously across the Pacific west, indicating
371 uniformly high vulnerability. However, changes in precipitation are much more spatially variable. The cold deserts
372 and Mediterranean California Ecoregions (Ecoregion level 2) have higher vulnerability, i.e., are more consistently
373 projected to experience changes in precipitation than has been observed since 1901 on a decadal basis. In contrast,
374 major portions of Arizona, Washington, Oregon, and California have areas with low vulnerability to change with
375 respect to precipitation. The PET vulnerability map is similar to the temperature vulnerability map, which is not
376 surprising since the Hamon (1961) method of calculating monthly PET uses temperature as the major input. The April
377 1 snow accumulation (snow water equivalent) vulnerability map shows high vulnerability in many mountainous areas
378 throughout the west. This seems to indicate that snow accumulation will change, particularly in transitional areas,
379 compared to the most snow prone areas of the West. S' is a measure of available water (excess water available for soil
380 infiltration or overland flow). The map for S' suggests that the Warm Desert and Marine West Coast Forest Ecoregions
381 are more likely to experience substantial changes in available water (i.e., high vulnerability) in the future. The FMI is
382 calculated from the ratio of PET and precipitation per Eq. (1). The FMI vulnerability map indicates that the Level 2
383 western Cordillera Ecoregion through northern Idaho (Fig. 1), a band of western Cordillera running north and south
384 through west of central Washington and Oregon (which includes portions of the Cascade Range), and portions of the
385 cold desert ecoregions in southeastern Washington and northwestern Arizona (Fig. 1) are more likely to see substantial
386 changes to the FMI. The regional time series analyses (below) provide more information about whether those areas
387 are expected to become wetter or drier. The seasonality vulnerability map identifies AUs that are likely to have changes
388 in seasonality. Portions of the western Cordillera Ecoregion (Fig. 1; which includes the Sierra-Nevada Mountains in
389 California, the Cascade Mountains in Washington and Oregon, and transitional terrain in Idaho) are projected to be
390 more vulnerable to changes in seasonality. Otherwise, large portions of the study area are not projected to be
391 vulnerable to changes for seasonality.

392 **3.2.1 Vulnerability of hydrologic landscapes**

393 Table 4 summarizes an analysis of the HL classifications of the most vulnerable AUs for each metric. For example,
394 75 % of the AUs identified as vulnerable for snow accumulation were classified as dry, moist, or wet, therefore very
395 wet, semi-arid, and arid AUs are less likely to be vulnerable to changes in snow accumulation. Likewise, 76 % of AUs
396 vulnerable to changes in seasonality had a spring seasonality during the 1971–2000 normal period. The physical
397 properties represented by the dominant HL classes in Table 4 could help determine how various climate vulnerabilities
398 are ultimately expressed. For example, vulnerability to changes in snow or FMI mostly occur in regions with wetter
399 climates (Moist, Wet, or Very Wet climate), with fall or spring Seasonality, in areas with low subsurface permeability.
400 This could result in increased precipitation, with quicker runoff in areas that currently have delayed release of water.

401 Similarly, areas vulnerable to changes in surface runoff are arid landscapes with winter seasonality and highly
402 permeable subsurface parent materials. This means that these changes in runoff could have a large impact on
403 subsurface recharge and, ultimately, baseflow.

404 **3.2.2 Case studies & locational time series**

405 Hydrologic vulnerability analyses have been performed for a total of 45 exposure areas of ecological, economic, or
406 social significance (Fig. 1 and Table 2; see Appendix A (Fig. A2)). The vulnerability index for each location is also
407 listed in Table 2 for each metric. Three case study locations that are of economic interest are explored in detail and
408 include Mt. Hood (Site #7), Willamette Valley (Site #9), Napa-Sonoma Valley (Site #28). During the normal period,
409 61 % of the 1867 km² Napa-Sonoma Valley had an MwHMH HL classification, thus much of the area was classified
410 as having a moist climate with winter seasonality, high subsurface permeability, mountain terrain, and high surface
411 permeability. Eighty-three percent of the 1234 km² Willamette Valley AUs had an HL code of WfHTH during the
412 normal period. Overall, the Willamette Valley had a wet climate, dominated by fall seasonality, high subsurface
413 permeability, transitional terrain, and high surface permeability. Table 2 indicates that 81 % of the 834 km² area
414 analyzed for Mt. Hood had an HL code of VsHMH (very wet climate with spring seasonality, high subsurface
415 permeability, mountainous terrain, and high surface permeability).

416 Figure 5 depicts line graphs of the historic and projected changes for the three case study locations (Mt. Hood (Site
417 #7), Willamette Valley (Site #9), Napa-Sonoma Valley (Site #28)). The number in the lower left corner of each graph
418 in Fig. 5 indicates the vulnerability index for the specific metric and location. For instance, precipitation at Mt. Hood
419 has a vulnerability index of ‘3’, which indicates that three of the climate projections exceed the threshold of two-
420 standard deviations from the historic mean.

421 The time series in Fig. 5 (and Fig. A2) illustrate the trend in average decadal temperature, precipitation, SWE, PET,
422 S’, climate, and seasonality of water surplus. Note that each future (2041–2070) climate projection is represented by
423 a single data point that characterizes the 2041 – 2070 30-year range and is connected in Fig. 5 to the 2001–2010
424 decade with a dotted red line. Additional figures for 42 other locations are provided in Appendix A (Fig. A2). Each
425 of the three example case studies is predicted to be warmer in the 2041–2070 future climate projections. Further, these
426 projected temperatures are almost always outside of the historic (1901–2010) temperature range, and so all locations
427 have high vulnerability with respect to future temperatures. None of the three case studies show a strong trend relating
428 to future precipitation projections. Mt. Hood appears to exhibit increasing precipitation since 1901, but there is no
429 evidence that the projected increases in precipitation are outside of historic behavior, and so the site has low
430 vulnerability for that metric. Napa-Sonoma and the Willamette Valley have low vulnerability for change in snow,
431 while Mt. Hood has high vulnerability for April 1 snow water equivalent in the 2041–2070 period. PET is calculated
432 directly from temperature and so its vulnerability is strongly correlated to temperature. There are no obvious trends in
433 S’ for the future projections in the three case studies; vulnerability of these sites for S’ is low to moderate. The FMI
434 projections for Napa-Sonoma Valley, the Willamette Valley, and Mt. Hood are outside of two-standard deviations of
435 historical trends in three to four out of ten of the projections (Table 2). In terms of seasonality, the vulnerability index

436 is equal to zero in the Willamette and Napa-Sonoma Valleys. For Mt. Hood, vulnerability is low, with all of the future
437 climate projections indicating that there will no longer be spring seasonality (the predominant historical season for
438 runoff). Only three climate models suggest that decadal seasonality would transition to winter seasonality, which has
439 not occurred since at least 1901.

440 **4 Discussion**

441 **4.1 Analyses of Retrospective and Projected Climate and Hydrologic Vulnerability**

442 Vulnerability maps (Fig. 4) were developed to facilitate long-term planning for stakeholders for assessing their risk to
443 climatic impacts. It is possible that ecosystems, businesses, and communities in areas mapped as vulnerable may
444 struggle to adapt to stresses imposed by future environmental conditions. As mentioned previously, the vulnerability
445 index offers no information about the directions of change projected by the ten different models. Further, the RCP 8.5
446 pathway was selected because it most closely resembles observed conditions (Schwalm et al., 2020).

447 The consistently projected high temperature vulnerability could lead to problems related to heat stress (e.g., human-
448 related physical and mental health issues), urban heat islands (particularly in areas with little tree cover), and other
449 temperature related problems (USGCRP, 2018). PET vulnerability would be problematic for agricultural systems,
450 forest disease, and sectors that are drought sensitive (USGCRP, 2018). Precipitation vulnerability maps are important
451 in specific areas with regards to flooding, landslides, and drought sensitivities. The vulnerability maps for snow
452 accumulation and S' (surplus water available for runoff or infiltration) show that the areas mapped as most vulnerable
453 for the two metrics are almost reversed, other than central Idaho and the coastal areas of California, Oregon, and
454 Washington. According to the snow vulnerability map, it appears that most areas that receive large amounts of snow
455 are projected to experience significant changes in future snow accumulation. In a related study on snow cover, Nolin
456 and Daly (2006) found that the areas with the warmest winter temperatures are most at risk of having no snow cover
457 in the future. Areas vulnerable for snow could impact not only the ski industry, but also water supply and streamflows,
458 while the surplus water availability (S') vulnerability metric relates more directly to streamflow and flooding. Most
459 of the study area is not vulnerable to changes in FMI (Fig. 4), which is an assessment of overall water availability,
460 although some areas are (the Willamette Valley in Oregon, east of Puget Sound in Washington, and the northern
461 panhandle in Idaho appear to be more vulnerable). The vulnerability map for seasonality (Fig. 4) shows that portions
462 of the Western Cordillera (Fig. 1) including the high Sierra-Nevada mountains in California, the Cascade mountains
463 in Oregon and Washington, and the mountainous areas in Idaho, have higher vulnerability indices, which indicates
464 susceptibility regarding water supply, flooding, and streamflows.

465 Our retrospective analysis of PRISM time series data provided an understanding of environmental conditions since
466 1901. We are aware of few that have used retrospective analyses to inform their mapping efforts (Deviney et al., 2006;
467 Kim et al., 2011; O'Brien et al., 2004), but are not aware of studies that have mapped resource vulnerability at a large
468 scale using such data. Our definition of vulnerability is based on agreement of climate models leading to conditions
469 that are outside of historic ranges. Our hypothesis is that systems having future climate conditions outside of the
470 historic range will not have the capacity to adapt to future conditions, and therefore are vulnerable. The vulnerability

471 issue is complicated by the fact that these vulnerability maps (Fig. 4) do not show how downstream areas could be
472 impacted by these changes.

473 These vulnerability factors may be of interest to resource managers and decision makers, some of who might consider
474 high vulnerability for a single metric to be problematic. Yet for others, the additive or multiplicative impacts of
475 numerous vulnerabilities may be of greater concern. For example, urban areas might be more impacted when
476 vulnerable to multiple metrics, whereas PET vulnerability could be detrimental to agricultural or forested areas.
477 Similarly, changes in seasonality from a snow dominated system to rain could have profound implications across
478 many sectors.

479 For this analysis, the 30-year normal climate conditions were compared to decadal climate conditions since 1901. In
480 addition, the 30-year normals for future projections (2041-2070) were compared to the historic range of decadal
481 climate data. While comparing 30-year normals in a decadal analysis might appear to be a discrepancy in the analysis,
482 the intention was to conservatively quantify vulnerability indices. Thirty-year normals exhibit less variability than
483 decadal averages or annual averages. By comparing decadal averages to the 30-year future climate normals, we are
484 not treating past data the same as future climate projections. However, the resulting vulnerability conclusions are
485 conservative, because if we had used decadal projections for future climate data, variability in the range of output
486 would have increased and our vulnerability indices could have increased for all parameters.

487 **4.2 Hydrologic Response and Hydrologic Landscape Classification**

488 The HL Class for an AU can provide insight into its hydrological response, given changes in the quantity (FMI) or
489 timing of surplus water (seasonality) on a landscape. Yet these factors only account for a portion of the water balance.
490 However, when moisture is available as surface runoff, it may infiltrate into the ground or act as surface runoff,
491 depending on the HL surface permeability class. Water may enter and flow through the subsurface layers (depending
492 on the HL subsurface permeability) towards a stream channel. If the water was directed as surface or subsurface runoff,
493 it may be transported more quickly in the downhill direction and into a stream channel depending upon the HL terrain
494 class, which governs steepness. As it relates to streamflow, the unique combination of the five HL characteristics
495 (climate, seasonality, surface permeability, subsurface permeability, and terrain) allows for the hydrologic response
496 to be assessed relative to changes in temperature and climate (Leibowitz et al., 2014; Patil et al., 2014). At its most
497 coarse application as it relates to this study, the transition from spring to winter seasonality for the Mt. Hood case
498 study would result in a shorter ski season with snow conditions that could be less ideal for winter sports. However,
499 this transition would also have many downstream impacts that could include flooding or habitat impacts. The HL
500 approach could also be used to determine any relationships between HL characteristics and hydrologic vulnerability,
501 while case studies can show how the HLVA could be useful.

502 **4.3 Case studies**

503 Case studies are useful for illustrating how future climate conditions may impact important economic and conservation
504 resources. It is necessary for a stakeholder to understand the parameters most important to their ecosystem, industry,
505 or resource of interest, so that they can utilize location specific information about their potential climatic impacts
506 (Glick et al., 2011; Lawler et al., 2010). In Fig. 5, case study examples (Mt. Hood (Site #7), Willamette Valley (Site
507 #9), Napa-Sonoma Valley (Site #28)) demonstrate how the HLVA can assist in understanding how climate can impact
508 important local water resources.

509 The wine and ski industries are important stakeholders in the western U.S. that may experience impacts from
510 hydrological changes. The Napa-Sonoma and Willamette Valleys are known for their vineyards and associated
511 wineries. Regarding their HL characteristics, they differ in their FMI class (Willamette is wet, whereas, Napa-Sonoma
512 is moist) and their seasonality (Willamette has a fall seasonality, while Napa-Sonoma has a winter seasonality). Due
513 to the importance of the pinot noir varietals in the Willamette Valley (Olen and Skinkis, 2018) and its temperature
514 sensitivity (Burakowski and Magnusson, 2012; Jones et al., 2010), local viticulturalists are likely more concerned with
515 changes in temperature than FMI. The Napa-Sonoma region is recognized for a variety of grape cultivars (Elliott-Fisk,
516 1993) that are less sensitive to temperature fluctuations (Jones et al., 2010). Both the Willamette Valley and Napa-
517 Sonoma have temperature vulnerability indices of ten out of ten, and both have FMI vulnerability indices of three out
518 of ten (Fig. 5). These indices suggest that both locations are projected to have future temperatures that are different
519 than historic temperatures. However, the Willamette Valley pinot noir grapes are more sensitive to temperature than
520 in the Napa and Sonoma Valleys. In addition, while both locations have the same FMI vulnerability indices, Fig. 5
521 illustrates that FMI projections for Napa-Sonoma are much more variable than for the Willamette Valley. Thus, there
522 is more uncertainty in the modeled water availability for Napa-Sonoma. These results suggest that a vintner growing
523 warm temperature grapes in the Willamette Valley may have more confidence in their investments relative to a vintner
524 in Napa-Sonoma, where there is more uncertainty regarding long-term water availability.

525 The skiing industry is economically important, and the impact between a high and low snowfall year for the State of
526 Oregon is \$38.1 million, while California is estimated to lose more than \$75 million in low snow years (Burakowski
527 and Magnusson, 2012). Mt. Hood is known for its winter snow sports and tourism and would be impacted differently
528 by the seven metrics than the Willamette and Napa-Sonoma case studies (Fig. 5). Thus, resource managers and
529 business leaders at Mt. Hood are likely more concerned about snow accumulation in their watershed than those in the
530 wine and grape industries (although grape grower's ability to irrigate may be impacted by snow accumulation in the
531 region). According to our analyses, Mt. Hood is generally characterized by having a spring seasonality and has a snow
532 vulnerability index of seven out of a maximum of ten. Also, the analysis of HL seasonality suggests some chance of
533 a shorter ski season due to the risk of spring runoff occurring earlier and imposing on the winter season. Even though
534 these conditions have occurred in the past (Fig. 5), this may be much more deleterious to the economics of the future
535 ski industry than it was in the 1900s, because it contributed much less to the historic economy (for additional examples
536 refer to Appendix A2).

537 **5 Summary and conclusions**

538 The hydrologic landscapes (HL) concept is useful for gaining a better understanding of hydrologic behavior at the
539 assessment unit and watershed scales across large geographic regions. By applying the HL concept to climatic and
540 vulnerability analyses, we provide a planning approach that allows resource managers to determine how vulnerable
541 they are to changes associated with climate that are important for a particular industry or application. Assessment of
542 expected hydrologic response based upon physical and climatic characteristics has the potential to offer further insight
543 into the idiosyncrasies of the nature of the threats faced by a stakeholder or industry across large geographic areas.
544 This will allow them to make informed decisions about the risk imposed by potential changes that could affect their
545 long-term planning efforts. The methodology also allows stakeholders to focus on specific areas of interest, which
546 provides the flexibility necessary for the information to be relevant across applications and sectors. By applying the
547 modified Wigington et al. (2013) approach across the western U.S., resource managers will be able to base
548 management decisions on assessments of climatic impacts of water resource vulnerability.

549 **6 Data availability**

550 The geospatial data files (Jones et al., 2020) will be uploaded to the GeoPlatform (<https://www.geoplatform.gov>) and
551 EPA Environmental Dataset Gateway (<https://edg.epa.gov>). Data cannot be made publicly available and the DOI link
552 cannot go activated until the paper is published per internal U.S. EPA policy.

553 **7 Code availability**

554 Authors may deposit code in a FAIR-aligned repository/archive upon final acceptance of the manuscript for
555 publication.

556 **8 Video abstract**

557 No video abstract is available at this time.

558 **9 Author contribution**

559 CJ and SL conceptualized the study with significant input from KS. CJ performed the formal analyses, investigation,
560 developed the methodologies (with input from SL, KS, and RC), managed the project, developed the model code,
561 performed the analyses, developed the final figures and tables, and wrote draft versions of the manuscript, and
562 incorporated co-author feedback into the final version of the manuscript. SL supervised the project and performed
563 project administration. RC contributed technical expertise regarding spatial data analyses and familiarity with
564 hydrologic landscapes data analyses. RC and LS developed the subsurface permeability datasets. PM and CW
565 provided the data and advice regarding the use of the future climate projections and the processing of those datasets.

566 **10 Acknowledgments**

567 We would like to thank James Markwiese, Mohammad Safeeq, Eric Sproles, and two anonymous reviewers for their
568 constructive feedback on the manuscript. We also appreciate Jim Wigington’s insight and input on early drafts of our
569 mapping products. We acknowledge the World Climate Research Programme's Working Group on Coupled
570 Modelling, which is responsible for CMIP, and we thank the climate modeling groups (listed in Table 1 of this paper)
571 for producing and making available their model output. For CMIP the U.S. Department of Energy's Program for
572 Climate Model Diagnosis and Intercomparison provides coordinating support and led development of software
573 infrastructure in partnership with the Global Organization for Earth System Science Portals. The information in this
574 document has been funded entirely by the U.S. Environmental Protection Agency, in part through an appointment to
575 the Internship/Research Participation Program at the Office of Research and Development, U.S. Environmental
576 Protection Agency, administered by the Oak Ridge Institute for Science and Education through an interagency
577 agreement between the U.S. Department of Energy and EPA, and also through Student Services Contract #EP-15-W-
578 000041. The views expressed in this paper are those of the authors and do not necessarily reflect the views or policies
579 of the U.S. Environmental Protection Agency. Any use of trade, firm, or product names is for descriptive purposes
580 only and does not imply endorsement by the U.S. Government.

581 **11 References**

- 582 Adger, W. N.: Vulnerability, *Glob. Environ. Chang.*, 16(3), 268–281, doi:10.1016/j.gloenvcha.2006.02.006, 2006.
- 583 Barnett, T. P., Adam, J. C. and Lettenmaier, D. P.: Potential impacts of a warming climate on water availability in
584 snow-dominated regions, *Nature*, 438(7066), 303–309, doi:10.1038/nature04141, 2005.
- 585 Battin, J., Wiley, M. W., Ruckelshaus, M. H., Palmer, R. N., Korb, E., Bartz, K. K. and Imaki, H.: Projected impacts
586 of climate change on salmon habitat restoration, *Proc. Natl. Acad. Sci. U. S. A.*, 104(16), 6720–6725,
587 doi:10.1073/pnas.0701685104, 2007.
- 588 Brekke, L. D., Kiang, J. E., Olsen, J. R., Pulwarty, R. S., Raff, D. A., Turnipseed, D. P., Webb, R. S. and White, K.
589 D.: Climate change and water resources management - A federal perspective: U.S. Geological Survey Circular 1331.,
590 2009.
- 591 Brown, R. D. and Mote, P. W.: The response of Northern Hemisphere snow cover to a changing climate, *J. Clim.*,
592 22(8), 2124–2145, doi:10.1175/2008JCLI2665.1, 2009.
- 593 Burakowski, E. and Magnusson, M.: Climate impacts on the winter tourism economy in the United States, *Natl.*
594 *Resour. Def. Counc.*, (December), 2012.
- 595 Bureau of Reclamation: Downscaled CMIP3 and CMIP5 Climate and Hydrology Projections: Release of Hydrology
596 Projections, Comparison with preceding Information, and Summary of User Needs, Denver, Colorado, U.S.A., 2014.

597 Comeleo, R. L., Wigington Jr., P. J. and Leibowitz, S. G.: Creation of a digital aquifer permeability map for the Pacific
598 Northwest (EPA/600/R-14/431), Corvallis, OR, USA., 2014.

599 Cook, B. I., Ault, T. R. and Smerdon, J. E.: Unprecedented 21st century drought risk in the American Southwest and
600 Central Plains, *Sci. Adv.*, 1(1), e1400082, doi:10.1126/sciadv.1400082, 2015.

601 Daly, C.: A new effort to update precipitation frequency maps for the United States., 2016a.

602 Daly, C.: PRISM Climate Group, Oregon State University, [online] Available from: <http://prism.oregonstate.edu>,
603 2016b.

604 Daly, C., Taylor, G. H., Gibson, W. P., Parzybok, T. W., Johnson, G. L. and Pasteris, P. A.: High-quality spatial
605 climate data sets for the United States and beyond, *Trans. ASAE*, 43(6), 1957–1962, doi:10.13031/2013.3101, 2000.

606 Dettinger, M., Redmond, K. and Cayan, D.: Winter orographic precipitation ratios in the Sierra Nevada—Large-scale
607 atmospheric circulations and hydrologic consequences, *J. Hydrometeorol.*, 5(6), 1102–1116, doi:10.1175/JHM-390.1,
608 2004.

609 Dettinger, M. D.: Climate change, atmospheric rivers, and floods in California - A multimodel analysis of storm
610 frequency and fagnitude changes, *J. Am. Water Resour. Assoc.*, 47(3), 514–523, doi:10.1111/j.1752-
611 1688.2011.00546.x, 2011.

612 Deviney, F. A., Rice, K. C. and Hornberger, G. M.: Time series and recurrence interval models to predict the
613 vulnerability of streams to episodic acidification in Shenandoah National Park, Virginia, *Water Resour. Res.*, 42(9),
614 doi:10.1029/2005WR004740, 2006.

615 Dhungel, S., Tarboton, D. G., Jin, J. and Hawkins, C. P.: Potential Effects of Climate Change on Ecologically Relevant
616 Streamflow Regimes, *River Res. Appl.*, 32(9), 1827–1840, doi:10.1002/rra.3029, 2016.

617 Elliott-Fisk, D. L.: Viticultural soils of California, with special reference to the Napa Valley, *J. Wine Res.*, 4(2), 67–
618 74, 1993.

619 ESRI: ArcGIS Desktop, [online] Available from: <http://www.esri.com/>, 2016.

620 Farley, K. A., Tague, C. and Grant, G. E.: Vulnerability of water supply from the Oregon Cascades to changing
621 climate: Linking science to users and policy, *Glob. Environ. Chang.*, 21(1), 110–122,
622 doi:10.1016/j.gloenvcha.2010.09.011, 2011.

623 Feddema, J. J.: A revised Thornthwaite-type global climate classification, *Phys. Geogr.*, 26(6), 442–466,
624 doi:10.2747/0272-3646.26.6.442, 2005.

625 Füssel, H. M.: Vulnerability: A generally applicable conceptual framework for climate change research, *Glob.*
626 *Environ. Chang.*, 17(2), 155–167, doi:10.1016/j.gloenvcha.2006.05.002, 2007.

627 Füssel, H. M. and Klein, R. J. T.: Climate change vulnerability assessments: An evolution of conceptual thinking,
628 *Clim. Change*, 75(3), 301–329, doi:10.1007/s10584-006-0329-3, 2006.

629 Glick, P., Stein, B. A. and Edelson, N. A., Eds.: Scanning the conservation horizon: A guide to climate change
630 vulnerability assessment, National Wildlife Federation, Washington D.C., USA., 2011.

631 Hamlet, A. F.: Assessing water resources adaptive capacity to climate change impacts in the Pacific Northwest Region
632 of North America, *Hydrol. Earth Syst. Sci.*, 15(5), 1427–1443, doi:10.5194/hess-15-1427-2011, 2011.

633 Hamon, W. R.: Estimating potential evapotranspiration, *J. Hydraul. Div.*, 87(3), 1961.

634 Hidalgo, H. G., Das, T., Dettinger, M. D., Cayan, D. R., Pierce, D. W., Barnett, T. P., Bala, G., Mirin, A., Wood, A.
635 W., Bonfils, C., Santer, B. D. and Nozawa, T.: Detection and attribution of streamflow timing changes to climate
636 change in the western United States, *J. Clim.*, 22(13), 3838–3855, doi:10.1175/2009JCLI2470.1, 2009.

637 Hijmans, R. J., Cameron, S. E., Parra, J. L., Jones, P. G. and Jarvis, A.: Very high resolution interpolated climate
638 surfaces for global land areas, *Int. J. Climatol.*, 25(15), 1965–1978, doi:10.1002/joc.1276, 2005.

639 Hill, R. A., Hawkins, C. P. and Carlisle, D. M.: Predicting thermal reference conditions for USA streams and rivers,
640 *Freshw. Sci.*, 32(1), 39–55, doi:10.1899/12-009.1, 2013.

641 Hill, R. A., Hawkins, C. P. and Jin, J.: Predicting thermal vulnerability of stream and river ecosystems to climate
642 change, *Clim. Change*, 125(3–4), 399–412, doi:10.1007/s10584-014-1174-4, 2014.

643 IPCC: Climate Change 2014: Impacts, Adaptation, and Vulnerability, edited by C. B. Field, V. R. Barros, D. J.
644 Dokken, K. J. Mach, M. D. Mastrandrea, T. E. Bilir, M. Chatterjee, K. L. Ebi, Y. O. Estrada, R. C. Genova, B. Girma,
645 E. S. Kissel, A. N. Levy, S. MacCracken, P. R. Mastrandrea, and L. L. White, Cambridge University Press, Cambridge,
646 UK and New York, NY, USA., 2014.

647 Jones, G. V., Duff, Andrew, A., Hall, A. and Myers, J. W.: Spatial analysis of climate in winegrape growing regions
648 in the western United States, *Am. J. Enol. Vitic.*, 61, 313–326, 2010.

649 Jung, I. W. and Chang, H.: Climate change impacts on spatial patterns in drought risk in the Willamette River Basin,
650 Oregon, USA, *Theor. Appl. Climatol.*, 108(3–4), 355–371, doi:10.1007/s00704-011-0531-8, 2012.

651 Kim, D. H., Yoo, C. and Kim, T. W.: Application of spatial EOF and multivariate time series model for evaluating
652 agricultural drought vulnerability in Korea, *Adv. Water Resour.*, 34(3), 340–350,

653 doi:10.1016/j.advwatres.2010.12.010, 2011.

654 Lawler, J. J., Tear, T. H., Pyke, C., Shaw, R. M., Gonzalez, P., Kareiva, P., Hansen, L., Hannah, L., Klausmeyer, K.,
655 Aldous, A., Bienz, C. and Pearsall, S.: Resource management in a changing and uncertain climate, *Front. Ecol.*
656 *Environ.*, 8(1), 35–43, doi:10.1890/070146, 2010.

657 Leibowitz, S. G., Wigington Jr., P. J., Comeleo, R. L. and Ebersole, J. L.: A temperature-precipitation-based model
658 of thirty-year mean snowpack accumulation and melt in Oregon, USA, *Hydrol. Process.*, 26, 741–759,
659 doi:10.1002/hyp.8176, 2012.

660 Leibowitz, S. G., Comeleo, R. L., Wigington Jr., P. J., Weaver, C. P., Morefield, P. E., Sproles, E. A. and Ebersole, J.
661 L.: Hydrologic landscape classification evaluates streamflow vulnerability to climate change in Oregon, USA, *Hydrol.*
662 *Earth Syst. Sci.*, 18(9), 3367–3392, doi:10.5194/hess-18-3367-2014, 2014.

663 Leibowitz, S. G., Comeleo, R. L., Wigington Jr., P. J., Weber, M. H., Sproles, E. A. and Sawicz, K. A.: Hydrologic
664 landscape characterization for the Pacific Northwest, USA, *J. Am. Water Resour. Assoc.*, 52(2), 473–493,
665 doi:10.1111/1752-1688.12402, 2016.

666 Luce, C. H. and Holden, Z. A.: Declining annual streamflow distributions in the Pacific Northwest United States,
667 1948–2006, *Geophys. Res. Lett.*, 36(16), 2–7, doi:10.1029/2009GL039407, 2009.

668 Mancosu, N., Snyder, R., Kyriakakis, G. and Spano, D.: Water Scarcity and Future Challenges for Food Production,
669 *Water*, 7(3), 975–992, doi:10.3390/w7030975, 2015.

670 Mann, M. E. and Gleick, P. H.: Climate change and California drought in the 21st century:, *Proc. Natl. Acad. Sci.*,
671 112(13), 3931–3936, doi:10.1073/pnas.1503667112, 2015.

672 Maurer, D. K., Lopes, T. J., Medina, R. L. and Smith, J. L.: Hydrogeology and hydrologic landscape regions of
673 Nevada, Carson City, NV., 2004.

674 McAfee, S. A.: Methodological differences in projected potential evapotranspiration, *Clim. Change*, 120(4), 915–930,
675 doi:10.1007/s10584-013-0864-7, 2013.

676 McKay, L., Bondelid, T., Dewald, T., Johnston, J., Moore, R. and Rea, A.: *NHDPlus Version 2: User Guide.*, 2012.

677 Mekonnen, M. and Hoekstra, A.: Four Billion People Experience Water Scarcity, *Sci. Adv.*, (2), 1–7,
678 doi:10.1126/sciadv.1500323, 2016.

679 Miller, D. A. and White, R. A.: A conterminous United States multi-layer soil characteristics data set for regional
680 climate and hydrology modeling, *Earth Interact.* 2 [online] Available from: <http://earthinteractions.org>, 1998.

681 Mock, C. J.: Climatic controls and spatial variations of precipitation in the western United States, *J. Clim.*, 9(5), 1111–
682 1124, doi:10.1175/1520-0442(1996)009<1111:CCASVO>2.0.CO;2, 1996.

683 Mote, P. W., Hamlet, A. F., Clark, M. P. and Lettenmaier, D. P.: Declining mountain snowpack in western North
684 America, *Bull. Am. Meteorol. Soc.*, 86(1), 39–49, doi:10.1175/BAMS-86-1-39, 2005.

685 National Intelligence Council: Global Water Security: Intelligence Community Assessment (ICA 2012-08),
686 Washington D.C., USA. [online] Available from: [https://www.dni.gov/files/documents/Special_Report_ICA_Global](https://www.dni.gov/files/documents/Special_Report_ICA_Global_Water_Security.pdf)
687 [Water Security.pdf](https://www.dni.gov/files/documents/Special_Report_ICA_Global_Water_Security.pdf), 2012.

688 Nelson, G. C.: Chapter 3. Drivers of Ecosystem Change: Summary Chapter, Island Press, Washington D.C., USA.,
689 2005.

690 Nijssen, B., O'Donnell, G. M., Hamlet, A. F. and Lettenmaier, D. P.: Hydrologic Sensitivity of Global Rivers to
691 Climate Change, *Clim. Change*, 50(1), 143–175 [online] Available from:
692 <http://www.springerlink.com/index/M24116121218031X.pdf> (Accessed 29 July 2011), 2001.

693 NOAA State Climate Extremes Committee: Climatic Extreme Records, NOAA Natl. Centers Environ. Inf. [online]
694 Available from: <http://www.ncdc.noaa.gov/extremes/scec/records> (Accessed 18 November 2018), 2016.

695 Nolin, A. W.: Perspectives on climate change, mountain hydrology, and water resources in the Oregon Cascades,
696 USA, *Mt. Res. Dev.*, 32, S35–S46, doi:10.1659/MRD-JOURNAL-D-11-00038.S1, 2011.

697 Nolin, A. W. and Daly, C.: Mapping “at risk” snow in the Pacific Northwest, *J. Hydrometeorol.*, 7, 1164–1171,
698 doi:10.1175/JHM543.1, 2006.

699 O'Brien, K., Leichenko, R., Kelkar, U., Venema, H., Aandahl, G., Tompkins, H., Javed, A., Bhadwal, S., Barg, S.,
700 Nygaard, L. and West, J.: Mapping vulnerability to multiple stressors: Climate change and globalization in India,
701 *Glob. Environ. Chang.*, 14(4), 303–313, doi:10.1016/j.gloenvcha.2004.01.001, 2004.

702 Olen, B. and Skinkis, P.: Vineyard Economics: Establishing and Producing Pinot Noir Wine Grapes in the Willamette
703 Valley, Oregon, Oregon State Univ., (October), 1–19 [online] Available from:
704 <https://agsci.oregonstate.edu/sites/agscid7/files/oaeb/pdf/aeb0060.pdf>, 2018.

705 Patil, S. D., Wigington Jr., P. J., Leibowitz, S. G. and Comeleo, R. L.: Use of hydrologic landscape classification to
706 diagnose streamflow predictability in Oregon, *J. Am. Water Resour. Assoc.*, 50(3), 762–776, doi:10.1111/jawr.12143,
707 2014.

708 Ramirez-Villegas, J. and Jarvis, A.: Downscaling global circulation model outputs: The delta method decision and
709 policy analysis working paper No. 1, Cali, Columbia. [online] Available from: [22/51](http://ccafs-</p>
</div>
<div data-bbox=)

710 climate.org/downloads/docs/Downscaling-WP-01.pdf, 2010.

711 Safeeq, M., Grant, G. E., Lewis, S. L., Kramer, M. G. and Staab, B.: A hydrogeologic framework for characterizing
712 summer streamflow sensitivity to climate warming in the Pacific Northwest, USA, *Hydrol. Earth Syst. Sci.*, 18(9),
713 3693–3710, doi:10.5194/hess-18-3693-2014, 2014.

714 Schwalm, C. R., Glendon, S. and Duffy, P. B.: RCP8.5 tracks cumulative CO2 emissions, *Proc. Natl. Acad. Sci.*,
715 117(33), 19656–19657, doi:10.1073/pnas.2007117117, 2020.

716 Siler, N., Roe, G. and Durran, D.: On the dynamical causes of variability in the rain-shadow effect: A case study of
717 the Washington Cascades, *J. Hydrometeorol.*, 14(1), 122–139, doi:10.1175/JHM-D-12-045.1, 2013.

718 Soil Survey Staff: Web Soil Survey, Nat. Resour. Conserv. Serv. USDA [online] Available from:
719 <http://websoilsurvey.nrcs.usda.gov/> (Accessed 18 May 2016), 2016.

720 Stratton, L., Comeleo, R. L., Leibowitz, S. G. and Wigington Jr., P. J.: Development of a digital aquifer permeability
721 map for the pacific southwest in support of the hydrologic landscape classification: Methods (EPA/600/R-16/063),
722 Corvallis, OR, USA. [online] Available from:
723 <https://nepis.epa.gov/Exe/ZyPDF.cgi/P100PB7N.PDF?Dockey=P100PB7N.pdf>, 2016.

724 Tague, C. and Grant, G. E.: A geological framework for interpreting the low-flow regimes of Cascade streams,
725 Willamette River Basin, Oregon, *Water Resour. Res.*, 40(4), 1–9, doi:10.1029/2003WR002629, 2004.

726 Tague, C. L., Choate, J. S. and Grant, G.: Parameterizing sub-surface drainage with geology to improve modeling
727 streamflow responses to climate in data limited environments, *Hydrol. Earth Syst. Sci.*, 17(1), 341–354,
728 doi:10.5194/hess-17-341-2013, 2013.

729 Tansel, B.: Hydrologic vulnerability and preventing domino effect consequences, *Hydrol. Curr. Res.*, 4(4), 10–11,
730 doi:10.4172/2157-7587.1000e11, 2013.

731 Taylor, K. E., Stouffer, R. J. and Meehl, G. A.: An overview of CMIP5 and the experiment design, *Bull. Am. Meteorol.*
732 *Soc.*, 93(4), 485–498, doi:10.1175/BAMS-D-11-00094.1, 2012.

733 Thompson, D. W. and Wallace, J. M.: Regional climate impacts of the Northern Hemisphere annular mode, *Science*,
734 293, 85–89, doi:10.1126/science.1058958, 2001.

735 Todd, M. J., Wigington Jr., P. J. and Sproles, E. A.: Hydrologic landscape classification to estimate Bristol Bay,
736 Alaska watershed hydrology, *J. Am. Water Resour. Assoc.*, 53(5), 1008–1031, doi:[https://doi.org/10.1111/1752-](https://doi.org/10.1111/1752-1688.12544)
737 [1688.12544](https://doi.org/10.1111/1752-1688.12544), 2017.

738 U.S. Environmental Protection Agency: A systematic approach for selecting climate projections to inform regional
739 impact assessments (Final). EPA/600/R-20/309, 2020. [online] Available from:
740 <https://cfpub.epa.gov/ncea/iclus/recordisplay.cfm?deid=349727>

741 U.S. Global Change Research Program: The United States National Climate Assessment. Uses of Vulnerability
742 Assessments for the National Climate Assessment. NCA Report Series, Volume 9., Washington D.C., USA. [online]
743 Available from: http://www.globalchange.gov/browse/reports?f%5B0%5D=field_report_year:171, 2011.

744 U.S. Global Change Research Program (USGCRP): Fourth National Climate Assessment, Washington D.C., USA.
745 [online] Available from: <https://www.globalchange.gov>, 2018.

746 Vano, J. A., Nijssen, B. and Lettenmaier, D. P.: Seasonal hydrologic responses to climate change in the Pacific
747 Northwest, *Water Resour. Res.*, 6(4), 1–18, doi:10.1002/2014WR015909, 2015.

748 Vorosmarty, C. J., Green, P., Salisbury, J. and Lammers, R. B.: Global water resources: Vulnerability from climate
749 change and population growth, *Science*, 289, 284–288, doi:10.1126/science.289.5477.284, 2000.

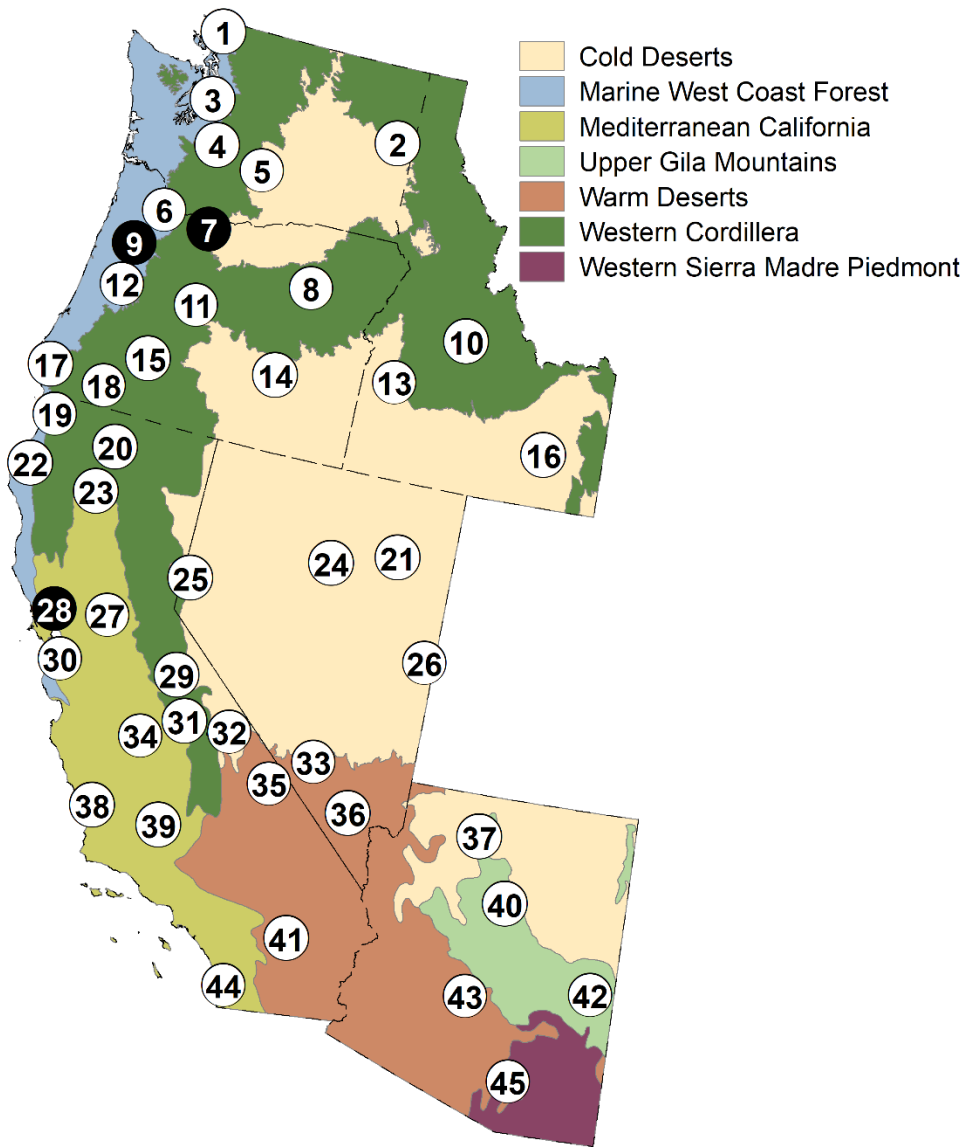
750 Watson, J. E. M., Iwamura, T. and Butt, N.: Mapping vulnerability and conservation adaptation strategies under
751 climate change, *Nat. Clim. Chang.*, 3(11), 989–994, doi:10.1038/nclimate2007, 2013.

752 Wigington Jr., P. J., Leibowitz, S. G., Comeleo, R. L. and Ebersole, J. L.: Oregon hydrologic landscapes: A
753 classification framework, *J. Am. Water Resour. Assoc.*, 49(1), 163–182, doi:10.1111/jawr.12009, 2013.

754 Winter, T. C.: The vulnerability of wetlands to climate change: a hydrologic landscape perspective, *J. Am. Water
755 Resour. Assoc.*, 36(2), 305–311, doi:10.1111/j.1752-1688.2000.tb04269.x, 2000.

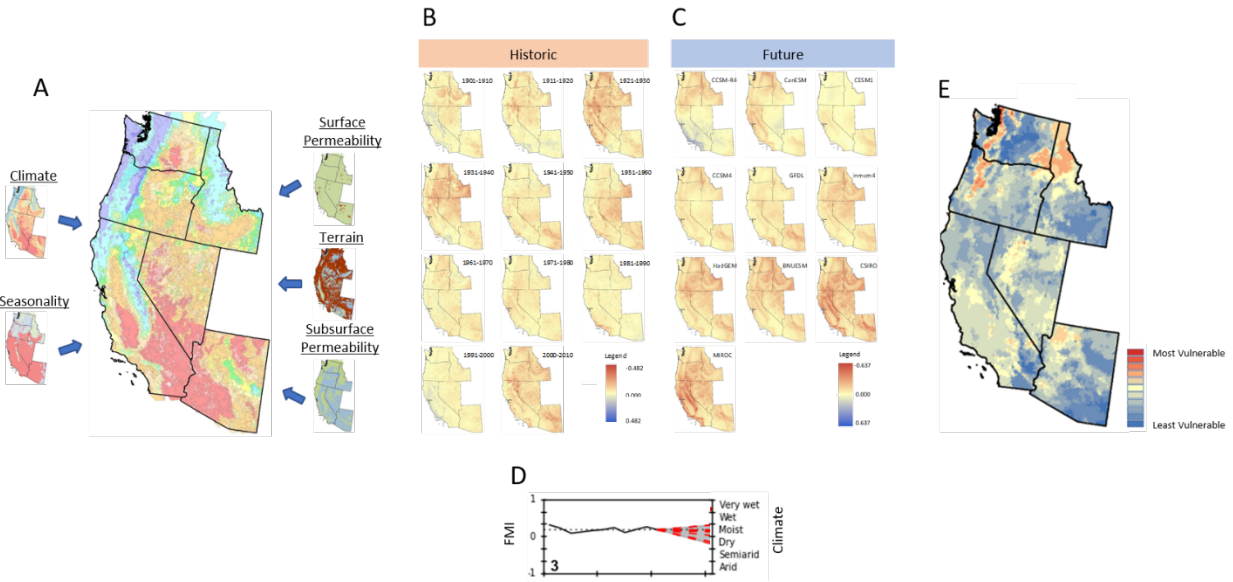
756 Winter, T. C.: The concept of hydrologic landscapes, *J. Am. Water Resour. Assoc.*, 37(2), 335–349, 2001.

757 Wolock, D. M., Winter, T. C. and McMahon, G.: Delineation and evaluation of hydrologic-landscape regions in the
758 United States using geographic information system tools and multivariate statistical analyses, *Environ. Manage.*, 34,
759 S71–S88, doi:10.1007/s00267-003-5077-9, 2004.



761

762 **Figure 1. Study area showing map with the six states of WA, OR, ID, CA, NV, and AZ. Also shown are the seven EPA Level**
763 **II Ecoregions (<https://www.epa.gov/eco-research/ecoregions-north-america>) and 45 locations identified by numbered**
764 **circles with three case study locations in black circles (Table 2). State boundaries are indicated by black dashed lines.**

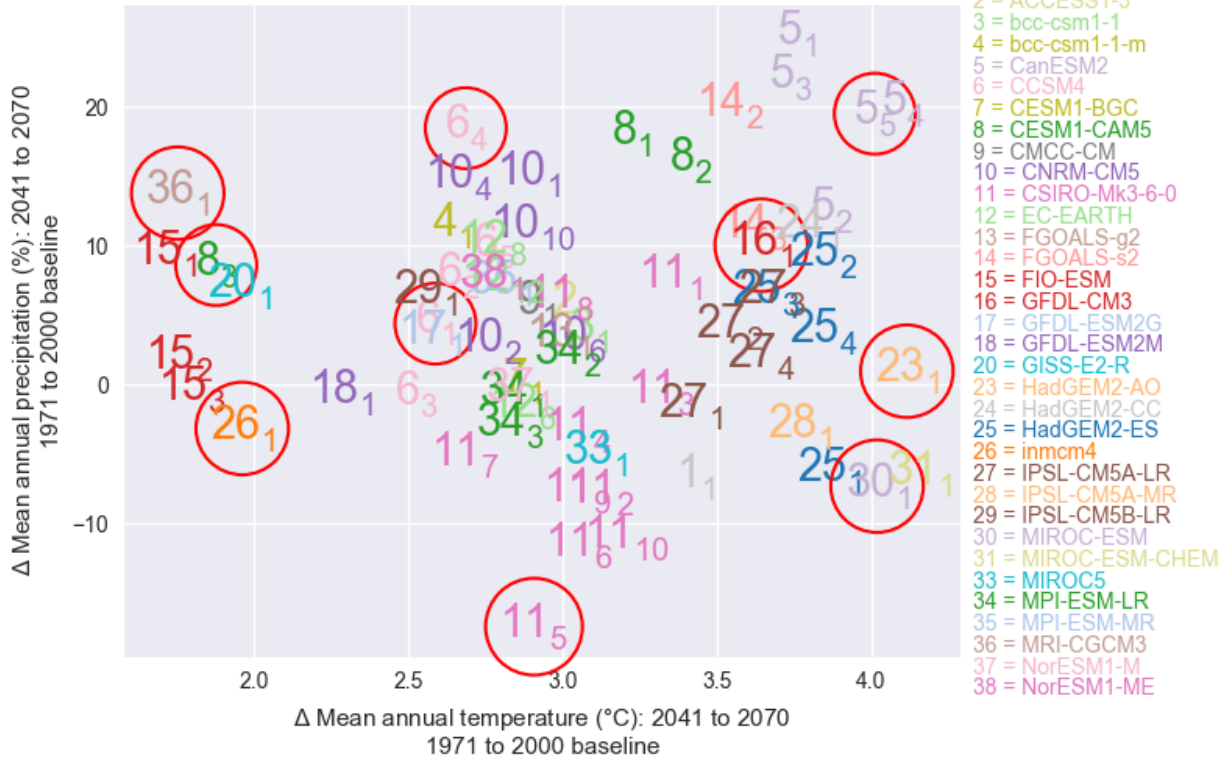


765

766 **Figure 2. Mapping of hydrologic vulnerability.** A) Hydrologic landscape map is developed for six western states using 1971-
 767 2000 normals for climate (Feddema Moisture Index; FMI) and seasonality, along with surface permeability, terrain, and
 768 subsurface permeability geophysical data. B) Historical decadal analysis is run from 1901 through 2010 for each of seven
 769 metrics: monthly temperature, precipitation, potential evapotranspiration, surplus water, snow water equivalent, FMI
 770 (shown), and seasonality. C) Future predicted behavior is estimated for each of the seven metrics, based on ten climate
 771 model projections (FMI shown). D) Vulnerability is then defined as the number of climate projections that lie outside of the
 772 historical two standard deviation threshold (example for FMI from Napa-Sonoma shown). E) Vulnerability values are then
 773 mapped for each metric across the six-state study area (FMI shown).

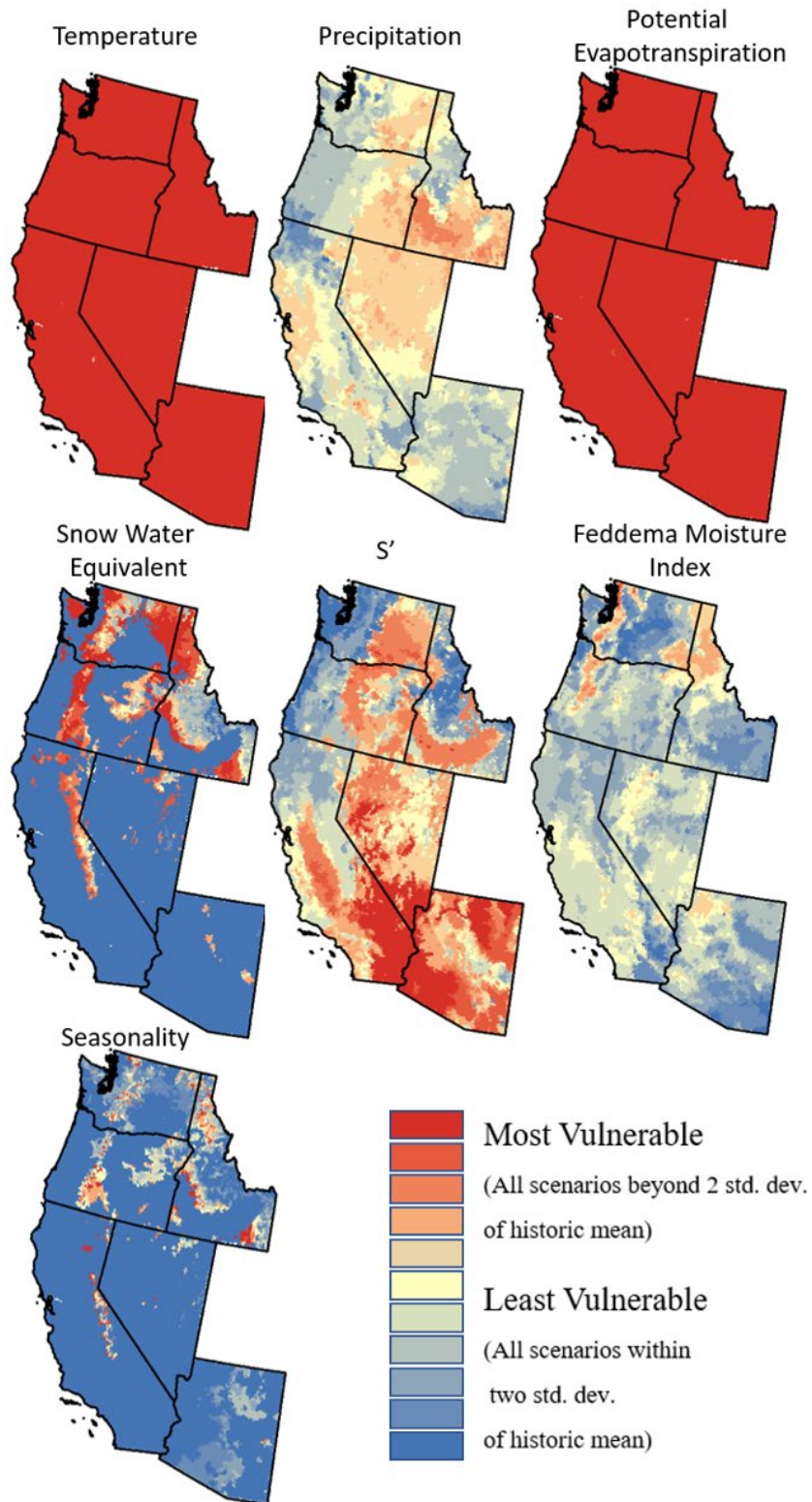
70 realizations of climate change from CMIP5 (BCSD)

Emissions Scenario: RCP85 Study area: AZ_CA_ID_NV_OR_WA



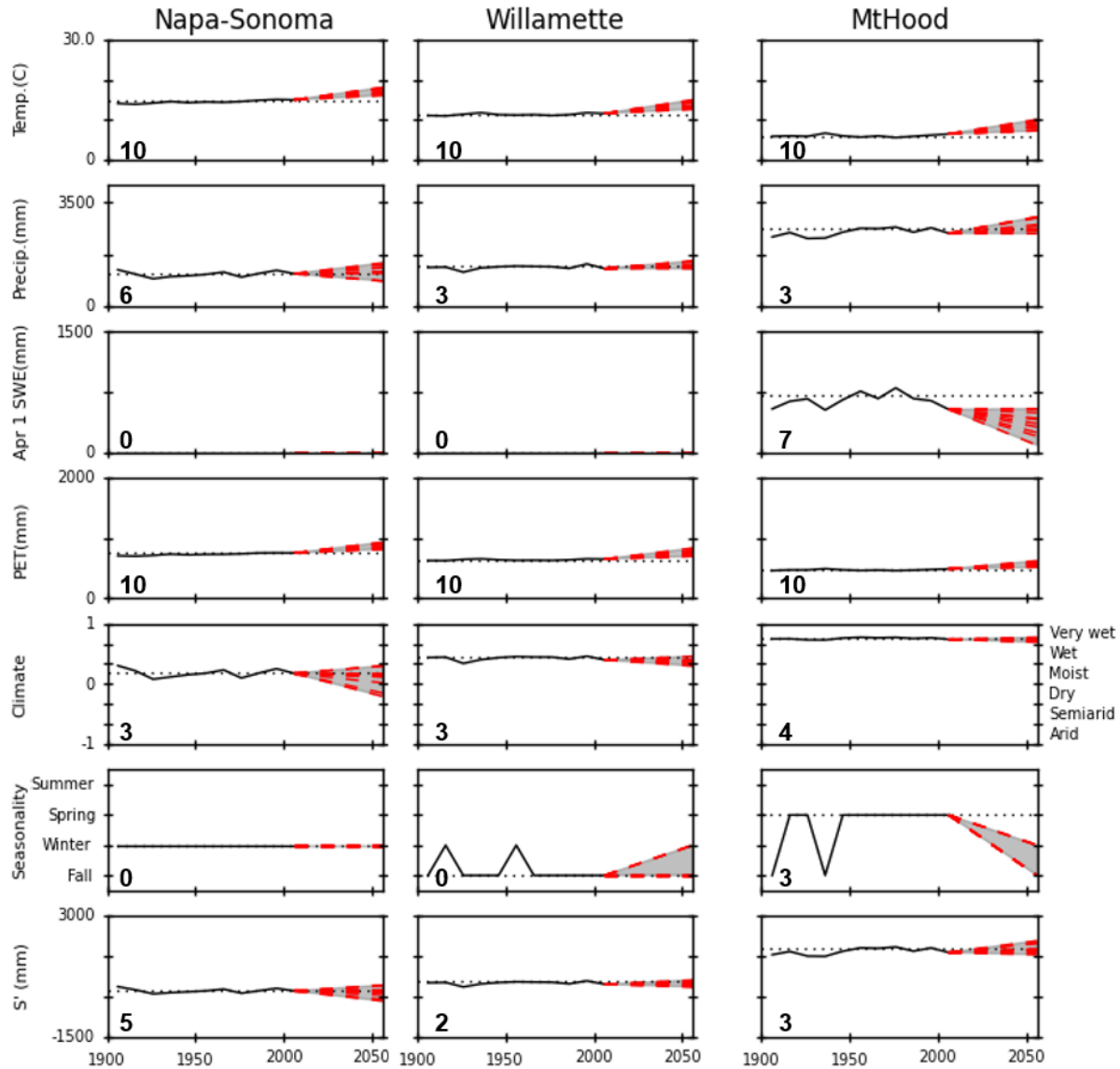
774
775
776
777
778
779

Figure 3. Scatterplot showing the range of mean temperature and precipitation projections for the 2041–2070 climate models across the study area. The circled data points identify the climate projections used in our analyses. Climate models are enumerated using the key to the right of the scatterplot. Subscripts denote the realization number of each unique projection. Legend colors are used to improve legibility where scatterplot symbols overlap.



780

781 **Figure 4. Vulnerability indices for temperature, precipitation, potential evapotranspiration, snow water equivalent (April**
 782 **1), S' (available water), Feddema Moisture Index, and seasonality. The least vulnerable locations are those projected to be**
 783 **within two-standard deviations of the historic (1901–2010) mean in all ten climate models.**



784

785 **Figure 5.** Time series of average decadal temperature, precipitation, snow (April 1 snow water equivalent (mm)), potential
 786 evapotranspiration (PET), climate (FMI), seasonality, and available water (S') for three specific locations in the western
 787 U.S. For the climate / FMI figures, the FMI values range from 1 to -1 (primary y-axis on the left), whereas the categorical
 788 version of the index ranges from arid to very wet (secondary y-axis on the right). Dotted black line represents the 1971–
 789 2000 base period; the dashed red line connects the 2001–2010 value to the 2041–2070 climate projections for each of the
 790 ten models. The gray shaded area represents the range of model projections. The number in lower left indicates the
 791 vulnerability index for the metric and location depicted in the associated graph.

792 **13 Tables**

793 **Table 1. CMIP5 Climate model summary for 2041–2070 precipitation and temperature data** (Bureau of Reclamation, 2014).

WCRP CMIP5 Climate Model	Model abbreviated name	Model realization used herein	Abbreviated name used in Figure 3 for realization
Canadian Earth System Model	CanESM2	r5i1p1	CanESM2
Community Climate System Model	CCSM4	r1i1p1	CCSM4
Community Climate System Model	CCSM4	r4i1p1	CCSM4-R4
Community Earth System Model	CESM1	r3i1p1	CESM1
Commonwealth Scientific and Industrial Research Organisation Mark 3.6	CSIRO-Mk3-6-0	r5i1p1	CSIRO
Geophysical Fluid Dynamics Laboratory Coupled Climate Model	GFDL-CM3	r1i1p1	GFDL
Hadley Global Environment Model	HadGEM2-AO	r1i1p1	HadGem
Institute for Numerical Mathematics Climate Model	INM-CM4	r1i1p1	inmem4
Model for Interdisciplinary Research on Climate	MIROC-ESM	r1i1p1	MIROC
Meteorological Research Institute	MRI-CGCM3	r1i1p1	MRI-CGCM3

794

795 **Table 2. Summary table for 45 study locations (sorted by decreasing latitude) providing numeric ID from Fig. 1, total analysis area, dominant HL class (representing**
796 **climate, seasonality, subsurface permeability, terrain, and surface permeability), percent area represented by dominant HL class, latitude and longitude of the center point**
797 **of the area, and vulnerability indices for temperature, precipitation, potential evapotranspiration (PET), surplus water (S'), snow water equivalent (snow), Feddema**
798 **Moisture Index (FMI), and seasonality.**

Site #	Name	Area (km ²)	Dominant HL Class*	% Dominant Area	Coordinates		Vulnerability Index						
					Lat.	Long.	Temp.	Pre cip.	PET	S'	Snow	FMI	Seasonality
1	Bellingham	212	WfLTH	99 %	48.77	-122.45	10	5	10	1	0	9	0
2	Spokane	592	DfHTH	80 %	47.64	-117.43	10	6	10	7	10	3	1
3	Seattle	669	WfLTH	78 %	47.60	-122.25	10	4	10	1	0	5	2
4	Mt Rainier	718	VsLMH	76 %	46.85	-121.79	10	4	10	2	7	4	2
5	Yakima	438	SfHTH	86 %	46.63	-120.60	10	3	10	6	0	0	0
6	Portland	932	WfHTH	67 %	45.53	-122.66	10	3	10	2	0	6	0
7	Mt. Hood	834	VsHMH	81 %	45.37	-121.70	10	3	10	3	7	4	3
8	Umatilla NF	2,147	MsLMH	29 %	44.87	-118.70	10	6	10	3	6	3	4
9	Willamette	1,234	WfHTH	83 %	44.84	-123.14	10	3	10	2	0	4	0
10	Challis NF	4,348	WsLMH	74 %	44.55	-114.75	10	6	10	0	3	2	0
11	Bend	948	SfHTH	68 %	44.21	-121.26	10	4	10	8	0	3	0
12	Eugene	523	WfHFH	64 %	44.10	-123.15	10	3	10	1	0	2	0
13	Boise	594	SwHTH	51 %	43.61	-116.24	10	8	10	8	0	2	0
14	Malheur NWR	1,355	SwHFH	69 %	43.27	-119.04	10	6	10	7	0	2	0
15	Crater Lake	1,721	WsHTH	45 %	42.98	-122.08	10	3	10	2	9	3	10

Site #	Name	Area (km ²)	Dominant HL Class*	% Dominant Area	Coordinates			Vulnerability Index					
					Lat.	Long.	Temp.	Pre cip.	PET	S'	Snow	FMI	Seasonality
16	Pocatello	349	DwHTH	45 %	42.88	-112.43	10	7	10	7	0	1	0
17	Siskiyou NF	926	VwLMH	100 %	42.36	-124.29	10	2	10	0	0	2	0
18	Medford	375	DfLTH	60 %	42.34	-122.89	10	1	10	5	0	2	0
19	Six Rivers	1,527	VwLMH	100 %	41.63	-123.79	10	2	10	2	0	4	0
20	Mt Shasta	956	WwHMH	49 %	41.36	-122.23	10	1	10	2	0	3	0
21	Ruby Mtn	1,132	DfLTH	44 %	40.68	-115.31	10	6	10	5	9	4	0
22	Arcata-Humboldt Co	2,511	WwLMH	63 %	40.62	-124.01	10	3	10	2	0	3	0
23	Redding	478	MwHTH	59 %	40.56	-122.38	10	2	10	2	0	2	0
24	Battle Mtn	902	SwLMH	75 %	40.09	-116.71	10	6	10	7	0	4	0
25	Reno	382	SwHTH	40 %	39.54	-119.80	10	4	10	7	0	3	0
26	Great Basin NP	38	MsLMH	100 %	39.01	-114.26	10	4	10	5	0	4	1
27	Sacramento	855	SwHFH	88 %	38.57	-121.39	10	6	10	7	0	3	0
28	Napa-Sonoma	1,867	MwHTH	61 %	38.37	-122.53	10	6	10	5	0	3	0
29	Yosemite NP	2,455	VsLMH	44 %	37.93	-119.55	10	4	10	4	9	3	0
30	San Francisco Bay	3,356	DwHMH	19 %	37.44	-122.29	10	6	10	5	0	5	0
31	Sierra NF	5,349	WwLMH	31 %	37.17	-119.05	10	4	10	4	0	2	0
32	High Sierras	2,239	WsLMH	32 %	37.15	-118.81	10	2	10	4	1	2	0

Site #	Name	Area (km ²)	Dominant HL Class*	% Dominant Area	Coordinates		Temp.	Pre cip.	Vulnerability Index				
					Lat.	Long.			PET	S'	Snow	FMI	Seasonality
33	Nevada Test Site	3,121	AwHMH	67 %	36.96	-116.22	10	5	10	10	0	4	0
34	Fresno	1,393	AwHFH	100 %	36.74	-119.91	10	5	10	8	0	4	0
35	Death Valley NP	7,862	AwHMH	50 %	36.45	-117.03	10	5	10	10	0	5	0
36	Las Vegas	977	AwHTH	65 %	36.23	-115.26	10	4	10	10	0	4	0
37	Grand Canyon NP	3,475	SwHMH	28 %	36.22	-112.11	10	4	10	10	0	6	0
38	San Luis Obispo	2,653	DwLMH	98 %	35.36	-120.63	10	4	10	4	0	4	0
39	Bakersfield	3,399	AwHFH	96 %	35.33	-119.14	10	4	10	9	0	4	0
40	Flagstaff	365	DwHMH	51 %	35.19	-111.60	10	3	10	4	0	4	0
41	Joshua Tree NP	2,599	AwLMH	68 %	33.92	-115.99	10	5	10	7	0	5	0
42	White Mtns	4,855	WfLMH	23 %	33.87	-109.53	10	4	10	3	0	3	0
43	Phoenix	2,304	AwHFH	63 %	33.52	-112.11	10	3	10	10	0	2	1
44	San Diego	1,276	SwLMH	37 %	32.90	-117.06	10	4	10	6	0	4	0
45	Tucson	1,838	AwHTH	62 %	32.19	-110.95	10	3	10	9	0	1	2

799 *Climate class (1st letter): V=very wet; W=wet; M=moist; D=dry; S=semiarid; A=arid

800 Seasonality class (2nd letter): f=fall; w= winter; s=spring; u=summer

801 Subsurface permeability class (3rd letter): L=low; H=high

802 Terrain class (4th letter): M=mountain; T=transitional; F=flat

803 Surface permeability class (5th letter): L=low; H=high

804 **Table 3. Percent of area of each HL category and classification within the six-state region (1971–2000)**

Category	Classification	Area (%)
Climate	Arid	21 %
	Semi-arid	34 %
	Dry	15 %
	Moist	9 %
	Wet	14 %
	Very wet	7 %
Season	Spring (AMJ ¹)	13 %
	Summer (JAS ²)	1 %
	Fall (OND ³)	24 %
	Winter (JFM ⁴)	63 %
Subsurface Permeability	Low	40 %
	High	60 %
Terrain	Flat	7 %
	Transitional	63 %
	Mountain	30 %
Surface Permeability	Low	2 %
	High	98 %

805 ¹AMJ: April, May, and June

806 ²JAS: July, August, and September

807 ³OND: October, November, and December

808 ⁴JFM: January, February, and March

809 **Table 4. Hydrologic landscape characteristics of assessment units identified as vulnerable (having a vulnerability index**
 810 **greater than 7 on a scale of 10) for each metric.**

		% Assessment units that share HL classification									
		Climate ¹		Seasonality ²		Subsurface Permeability ³		Terrain ⁴		Surface permeability ³	
Vulnerability Parameter	Temperature	70	D, S, or A	87	f or w	60 %	H	93	M or T	98 %	H
	Precipitation	72	D or S	79	f or w	71 %	H	97	M or T	98 %	H
	PET	70	D, S, or A	87	f or w	60 %	H	93	M or T	98 %	H
	Surplus water (S')	92	A or S	79	w	75 %	H	87	M or T	99 %	H
	Snow water equivalent (SWE)	75	D, M, or W	87	f or s	53 %	L	82	M	100 %	H
	FMI	71	V or W	65	f	75 %	L	75	M	100 %	H
	Seasonality	75	W or M	76	s	51 %	H	83	M	99 %	H

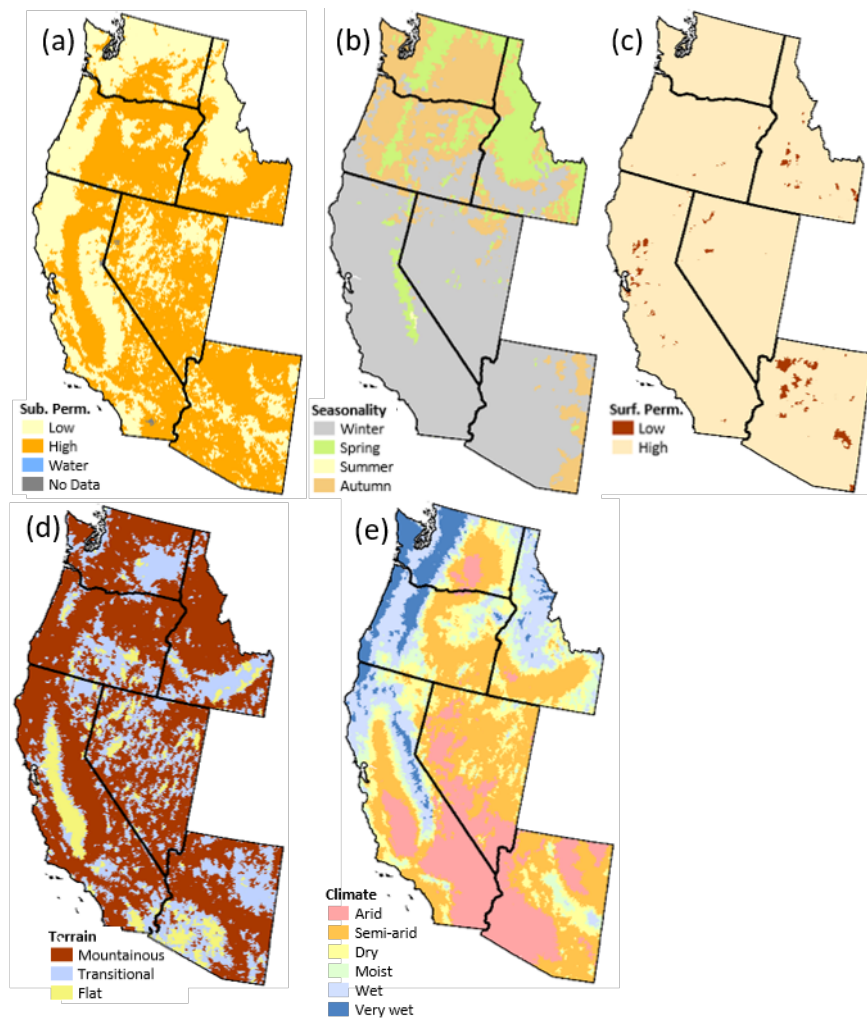
811 ¹A=arid, S=semiarid, D=dry, M=moist, W=wet

812 ²f=fall, w=winter, s=spring

813 ³L=low, H=high

814 ⁴T=transitional, M=mountainous

815

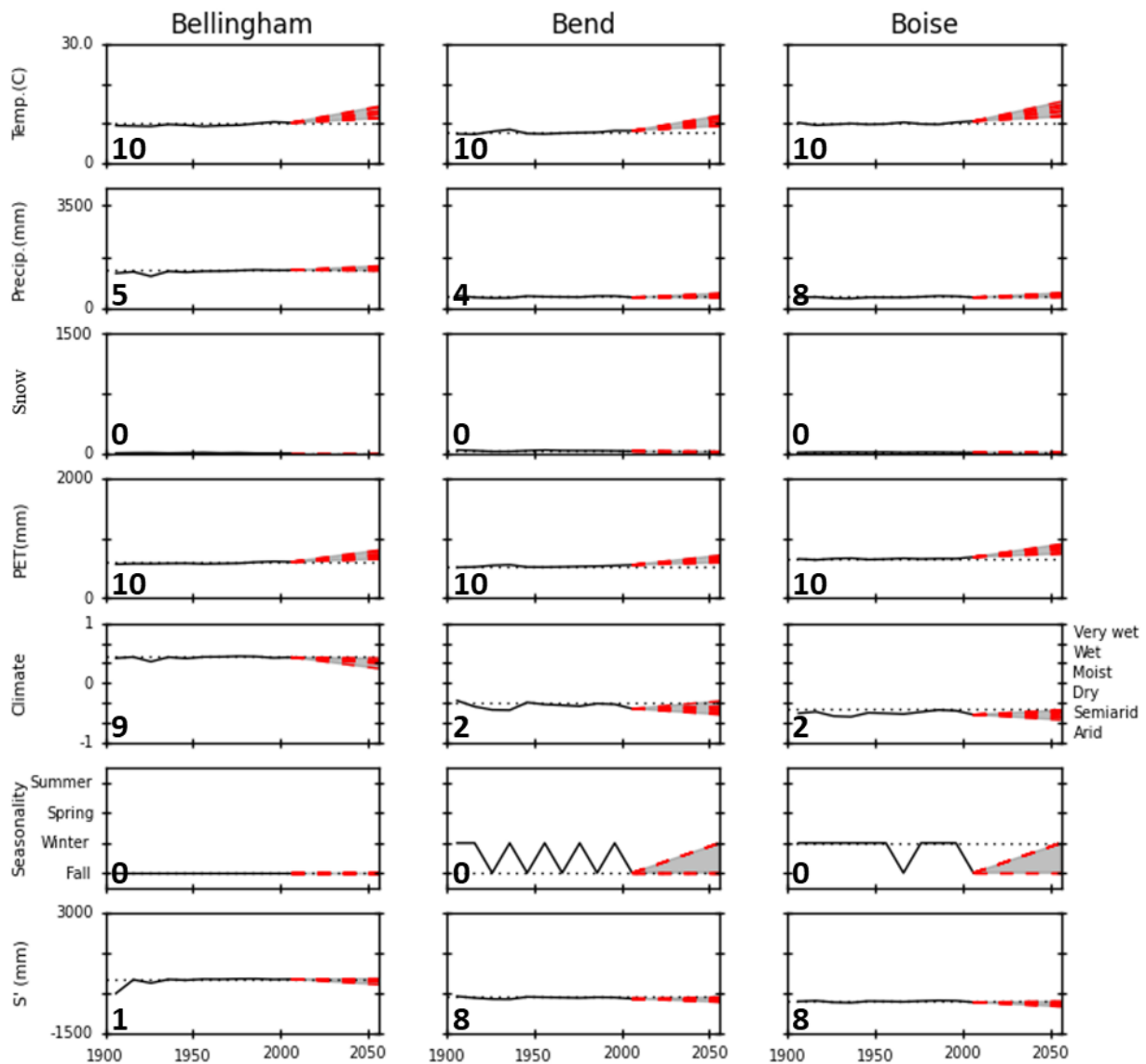


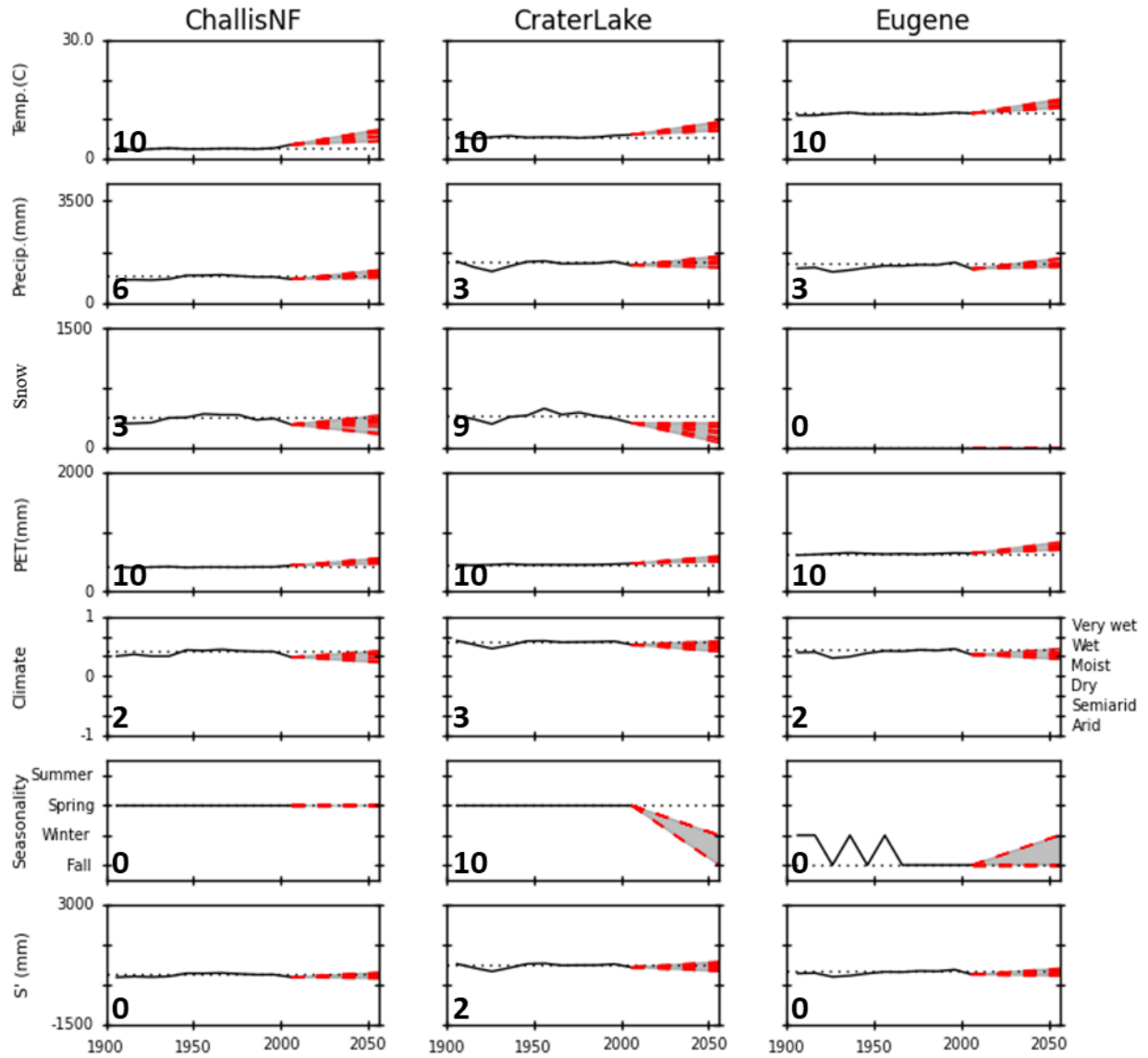
817

818 **Figure A1. Component Hydrologic Landscape maps of Washington, Idaho, Oregon, California, Nevada, and Arizona were**
 819 **used in the analysis of the HLVA indices [(a) Subsurface Permeability, (b) Seasonality of precipitation surplus, (c) Surface**
 820 **permeability, (d) Climate, and (e) Terrain]. Notes: The seasonality map for the PNW has been updated from the original**
 821 **Leibowitz et al. 2016 HL map, as we separated their winter seasonality into two seasons (winter and fall).**

822 **Figure A2**

823 **Time series of average decadal temperature, precipitation, snow (April 1 snow water equivalent), potential**
 824 **evapotranspiration (PET), climate (FMI), seasonality, and available water (S') for 45 specific locations in the western U.S.**
 825 **For the climate / FMI figures, the FMI values range from 1 to -1 (primary y-axis on the left), whereas the categorical version**
 826 **of the index ranges from arid to very wet (secondary y-axis on the right). Dotted black line represents the 1971–2000 base**
 827 **period; the dashed red line connects the 2001–2010 value to the 2041–2070 climate projections for each of the ten models.**
 828 **The gray shaded area represents the range of model projections. The number in lower left indicates the HLVA vulnerability**
 829 **index for the metric and location depicted in the associated graph. Note that Oregon, Washington, and Idaho locations are**
 830 **displayed first in alphabetical order and are followed by those of California, Nevada, and Arizona.**





832

833

